JGR Solid Earth

RESEARCH ARTICLE
10.1029/2020JB021079

Special Section:
Ophiolites and Oceanic Lithosphere, with a focus on the Samail ophiolite in Oman

Uplift and Exposure of Serpentinized Massifs: Modeling Differential Serpentinite Diapirism and Exhumation of the Troodos Mantle Sequence, Cyprus

Aled D. Evans[1], Damon A. H. Teagle[1], Dave Craw[2], Timothy J. Henstock[1], and Ismael Himar Falcon-Suarez[3]

[1]School of Ocean and Earth Science, National Oceanography Centre Southampton, University of Southampton, Southampton, UK, [2]Department of Geology, University of Otago, Dunedin, New Zealand, [3]Marine Geoscience, National Oceanography Centre, Southampton, UK

Key Points:

- Coupled isostatic uplift-erosion modeling explains the outcrop pattern of the Troodos mountains
- Contrasting extents of serpentinization within the Mantle Sequence induced differential exhumation between two serpentinite domains
- Uplifted serpentinite massifs worldwide, reflect the relative contributions of serpentinization-induced isostasy and tectonics

Supporting Information:

Supporting Information may be found in the online version of this article.

Correspondence to:

A. D. Evans,
A.Evans@southampton.ac.uk

Citation:

Evans, A. D., Teagle, D. A. H., Craw, D., Henstock, T. J., & Falcon-Suarez, I. H. (2021). Uplift and exposure of serpentinized massifs: Modeling differential serpentinite diapirism and exhumation of the Troodos Mantle Sequence, Cyprus. *Journal of Geophysical Research: Solid Earth*, *126*, e2020JB021079. https://doi.org/10.1029/2020JB021079

Received 5 OCT 2020
Accepted 18 MAY 2021

Abstract Serpentinized mantle peridotites form prominent mountains, including the highest elevations of the Troodos ophiolite in Cyprus (Mount Olympus, 1,952 m), but to date, only qualitative mechanisms have been proposed to explain the uplift of mantle rocks to high altitudes. Serpentinization reactions between mantle rocks and water result in profound changes to the rheology and physical properties of peridotites including significant density reduction (~900 kg/m^3). Field observations, density measurements, and isostatic uplift and erosional modeling provide new constraints on the contribution of serpentinization to the uplift of the Troodos Mantle Sequence. Different serpentinization styles have resulted in two distinct serpentinite domains with contrasting densities. Our modeling shows that the Troodos Mountains can form within the geologically constrained uplift time frame (~5.5 Myr) exclusively through partial serpentinization reactions. We interpret the serpentinite domains as two nested diapirs that formed due to different extents of serpentinization and density reduction. Differential uplift and exhumation have decoupled the two serpentinite diapirs from the originally overlying ocean crustal rocks. Once at high altitudes the incursion of meteoric water reinforced coupled deformation-alteration-recrystallization processes in the shallow subsurface producing a localized low density completely serpentinized diapir. A second decoupling between the contrasting serpentinite diapirs results in localized differential uplift and exhumation, extruding deep materials to the east of Mount Olympus. Application of our modeling to other serpentinite massifs (e.g., St. Peter and St. Paul Rocks, New Idria, California) highlights the contribution of isostasy to the uplift of serpentinized massifs.

1. Introduction

Partially serpentinized mantle rocks form prominent topographic features in numerous locations on Earth, both on land and in the oceans, for example, Ronda Massif, Spain, Dun Mountain, New Zealand, and the Atlantis Massif on the Mid-Atlantic Ridge. Although some of these exposures can be explained by dynamic tectonics, other features require different explanations.

Serpentinization reactions between water and mantle rocks dramatically change high density (3,300 kg/m^3), relatively strong, anhydrous, low permeability, mantle peridotites into low density (2,400 kg/m^3), weak serpentinites, inducing up to 40% volume expansion (Macdonald & Fyfe, 1985; Toft et al., 1990). The reduction in bulk density results in isostatic uplift, that together with serpentinite diapirism, has been proposed to have led to the exposure of serpentinized mantle peridotites at moderate to high altitudes on land in the Troodos Massif, Cyprus (e.g., Gass, 1977; Gass & Masson-Smith, 1963; Moores & Vine, 1971) and the New Idria Massif, California (e.g., Coleman, 1996; Tsujimori et al., 2007), and in the oceans forming the emergent St. Peter and St. Paul Rocks (e.g., Campos et al., 2010).

Here, we investigate the uplift and exposure of the Troodos Massif of Cyprus and combine field observations with new density measurements and isostatic and differential erosion rate calculations to test whether serpentinization can form the Troodos Massif. We document the contrasting manifestations of serpentinization in the exhumed Mantle Sequence and calculate whether the isostatic consequences of the density and rheological differences can develop the distinctive but hitherto poorly explained outcrop pattern of this

iconic geological terrane. We further apply our mechanistic uplift model to other settings and demonstrate the universality of our approach.

2. Mantle Peridotite Massifs and Serpentinite Diapirism

Although mantle peridotite is the most common rock type on Earth, surface exposures of mantle rocks are relatively rare and predominantly strongly to completely altered by serpentinization reactions (e.g., Kelemen et al., 2011). Major outcrops of mantle peridotites are generally limited to ophiolites and oceanic core complexes. A component of isostasy is an inevitable consequence of serpentinization reactions, but serpentinite diapirism is not ubiquitously invoked in every manifestation of serpentinization. It is unclear whether serpentinite diapirism is overlooked or if subsequent deformation has obliterated geological evidence (e.g., Gass, 1977). Previously reported occurrences of serpentinite diapirism indicate a diverse spectrum of diapiric modes rather than a single mechanism. Here, we briefly outline some previously reported examples of serpentinite diapirism that represent this spectrum of occurrence.

2.1. Examples of Serpentinite Diapirism Associated With Isostatic Uplift

2.1.1. Partially Serpentinized Serpentinite Diapirs

Isolated mantle peridotite massifs have long been associated with variable extents of serpentinization (e.g., Darwin, 1835), and their differential uplift relative to the surrounding seafloor has been proposed to occur due to the lower density of serpentine (e.g., Boillot et al., 1980; Bonatti, 1976; Hess, 1954). Isostatic uplift as a result of density-reduction from partial serpentinization reactions, in combination with transpressional tectonics, has been previously invoked to explain isolated mantle peridotite massifs along oceanic fracture zones (e.g., Bonatti, 1978; Campos et al., 2010; Kil et al., 2010). For example, associated with the St. Paul and St. Peter Fracture Zones (0.6°N and 2.5°N) in the equatorial Atlantic, the St. Peter and St. Paul Rocks archipelago (Campos et al., 2010) is primarily composed of variably serpentinized mylonitized mantle peridotite (e.g., Campos et al., 2005, 2010; Hekinian et al., 2000; Melson et al., 1972). These islands are only the emergent portion of the much larger (~90 × ~20 km^2 at 3,000 m bsl) submerged variably serpentinized North Ridge mantle peridotite massif that rises from abyssal depths (~4,000 mbsl, Campos et al., 2010; Hekinian et al., 2000; Maia et al., 2016). Radiometric dating suggests that the archipelago only became emergent in the past ~6,500 years, with uplift on-going at a minimum uplift rate of >1.5 mm/yr (Campos et al., 2010).

2.1.2. Completely Serpentinized Serpentinite Diapirs

Discreet occurrences of completely serpentinized mantle peridotites have previously been interpreted as distinct serpentinite diapirs. A key characteristic and composition of these surficial serpentinite extrusions is a low-density, mélange-like serpentinite breccia assemblage, where strongly altered and completely serpentinized peridotite clasts are hosted in a finely comminuted serpentinite gouge. These easily erodible materials are commonly associated with elevated topography, and consequently high uplift rates are often inferred to maintain the high relief of these easily erodible serpentinite extrusions. Examples that occur near the San Andreas Fault, California include the ~5 km^2 1,027-m-high Table Mountain (Dickinson, 1966; Moore & Rymer, 2007) and the ~100 km^2 New Idria Massif (1,605 m, Coleman, 1996; Tsujimori et al., 2007). Both features are interpreted as completely serpentinized serpentinite diapirs. A rapid uplift rate of ~4 mm/yr is estimated from the relative displacement of sedimentary indicators (Coleman, 1996). This rapid uplift rate is balanced by an inferred high erosion rate of ~4 mm/yr that indicates ~17 km^3 has been removed from the New Idria serpentinite diapir (Coleman, 1996; Mumpton & Thompson, 1975). The rapid uplift rate (~4 mm/yr) is significantly greater than the estimated regional uplift rate for the Coast Ranges (~1 mm/yr; Page et al., 1998), implying differential uplift and exhumation between the New Idria serpentinite diapir and surrounding area simultaneously producing and maintaining ~1,000 m of elevated relief.

2.2. Examples of Serpentinite Diapirism Not Associated With Isostatic Uplift

The large (~30 km in diameter, ~2 km high) submerged serpentinite mud volcanoes of the Mariana forearc have previously been referred to as examples of serpentinite diapirism (e.g., Fryer et al., 1985, 1992; Ishii et al., 1992). Although these features contain clasts of strongly serpentinized mantle peridotite and

metabasalts, some with sub-blueschist assemblages, these mud volcanoes are predominantly built from multiple effusions of unconsolidated serpentinite muds. These muds are, inferred to be produced by progressive interactions between serpentinized peridotites from the mantle wedge of the upper plate and subducting slab-derived fluids. Over-pressured mud-rich fluids then rise up steeply dipping faults before episodically erupting onto the seafloor (e.g., Fryer, 2012; Mottl et al., 2004). Fluid mass transfer resulting in multiple episodes of mud-eruption have built up these serpentinite seamounts (Fryer, 2012) as opposed to isostatic responses resulting directly from serpentinization reactions. These mud volcanoes therefore differ from other completely serpentinized peridotite diapirs as they are not associated with surface uplift.

3. The Troodos Massif

Here, we investigate the uplift of the Troodos Massif, one of the world's best-preserved, least deformed, and most complete ophiolites (Gass, 1968). The Troodos mountains expose ocean crust and upper mantle rocks that formed ~90–92 Ma at some form of supra-subduction zone spreading ridge in the Neo-Tethyan Ocean (Moores & Vine, 1971; Moores et al., 1984; Mukasa & Ludden, 1987; Pearce et al., 1984). The ~90-km-long and ~30-km-wide ophiolitic sequence crops out as an elliptical bullseye-patterned welt, with the stratigraphically deepest rocks, partially serpentinized mantle peridotites, forming the highest elevation of the Troodos mountains (Mount Olympus, 1,952 m asl). This Mantle Sequence is surrounded by an eroded anticlinal dome comprising concentric annuli of gabbroic and ultramafic cumulate rocks, sheeted dikes, lavas, and submarine sediments that crop out at progressively lower altitudes around the slopes of the massif (Figure 1a).

Unlike other ophiolites, such as the Samail ophiolite of Oman (e.g., Hacker et al., 1996; Searle & Cox, 1999), the Troodos ophiolite was not obducted onto a continental margin soon after its formation and there is no metamorphic sole to the massif. In contrast, significant uplift of the Troodos ophiolite has occurred since 5.5 Ma (e.g., McCallum, 1989; Poole & Robertson, 1991, 1998; Robertson, 1977; Rouchy et al., 2001; Stow et al., 1995) and it is qualitatively inferred that the exposure of the Troodos massif results from the serpentinization of peridotites from the mantle below the ocean crustal rocks of the ophiolite (Gass & Masson-Smith, 1963; Moores & Vine, 1971; Robertson, 1977, 1998).

The initial serpentinization of the Troodos Mantle Sequence is commonly invoked to have occurred due to the collision of the Eratosthenes Seamount continental block with the Cyprean trench to the south of Cyprus that has stalled the northward subduction of the African plate (Ergün et al., 2005; Robertson, 1998). It is proposed that this has resulted in the focused upwelling into the overlying mantle wedge of hydrous fluids generated by the dewatering of partially subducted marine sediments and ocean lithosphere, inducing and focusing serpentinite diapirism onto the Mount Olympus region (Gass, 1977; Moores & Vine, 1971; Robertson, 1977, 1998). The best estimates for the dip of the subducting plate in the Cyprean arc are between ~13° and ~33° (Feld et al., 2017; Mackenzie et al., 2006) with the top of the down-going slab lying between ~13 and ~40 km below Mount Olympus. Oxygen and hydrogen isotopic measurements of the Troodos Mantle Sequence indicate that discrete portions of the Mantle Sequence have interacted with meteoric and "oceanic-like" waters (Magaritz & Taylor, 1974; Nuriel et al., 2009), suggesting the progressive and episodic serpentinization of the Mantle Sequence is likely on-going.

Other mechanisms have also been suggested to explain the geometry of the Troodos Massif including Cretaceous ridge-related serpentine diapirism (Schuiling, 2011) and Cretaceous ridge-related detachment faulting (Nuriel et al., 2009). Recent regional structural analysis downplays the importance of serpentinization and suggests uplift can be generated solely by Miocene to present-day convergence across the Cyprean subduction zone (Ring & Pantazides, 2019).

3.1. The Troodos Massif Mantle Sequence

The highest part of the Troodos Massif (Figure 1a) comprises a ~200 km^2 central region at moderate altitude (>1,200 m) comprising mantle peridotite and surrounding gabbro, characterized by gentle hillslopes and relatively wide, shallow valleys, although the boundary between the gabbros and peridotites is commonly faulted with steep relief in places. In contrast, the surrounding Sheeted Dike Complex is exposed in steep-sided ridges up to ~1,000 m altitude that are deeply incised, with the encompassing Extrusive

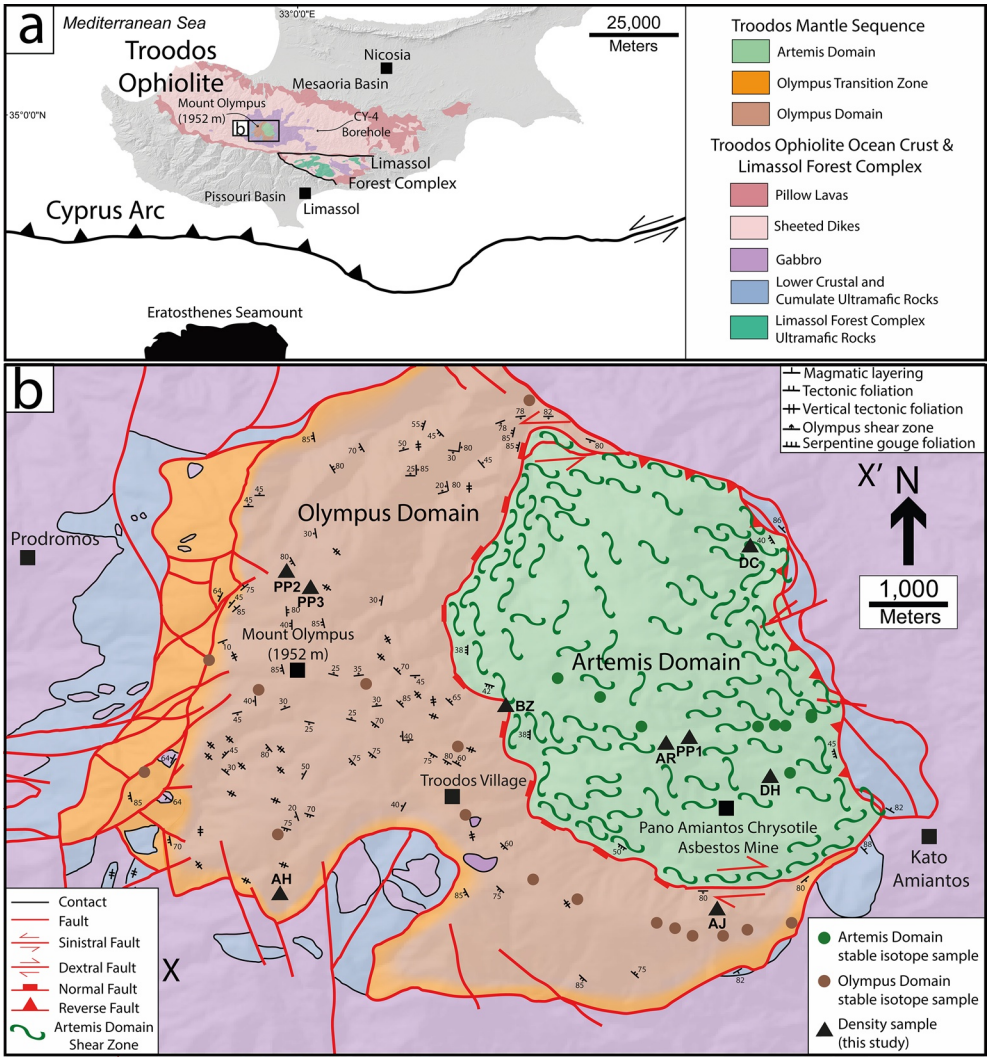

Figure 1. (a) Geological map of the Troodos ophiolite with the bullseye geometry of the Mantle Sequence highlighted along with the Limassol Forest Complex terrane, the Cyprus arc, and northernmost portion of the Eratosthenes Seamount. (b) Geological map of the Troodos Mantle Sequence, adapted and updated from Wilson (1959). *X*–*X*′ shows line of cross-section (see Supporting Information for entire line of cross-section; Figure 2). Density sample locations shown as are sample locations for published oxygen and hydrogen stable isotope analyses by Magaritz and Taylor (1974), Heaton (1976), and Nuriel et al. (2009).

Sequences and circum-Troodos sediments occurring at lower altitudes in gently dipping outcrops best exposed in river canyons.

The Mantle Sequence of the Troodos Massif can be subdivided into two discrete regions (Figure 1b): (a) an arcuate western zone of partially (~50%–~70%) serpentinized tectonized harzburgites with minor dunites, referred to here as the Olympus domain, juxtaposed by faults against (b) an eastern ~5 km diameter, subcircular region of completely serpentinized peridotite blocks in a sheared matrix of serpentine breccia (Figure 2), here named the Artemis domain. The Artemis domain rocks have previously been referred to as the Smash zone (Wilson, 1959) or The Serpentine (Gass & Masson-Smith, 1963), or the remobilized serpentinite plug (Moores & Vine, 1971).

The Cr-number (Cr/Cr + Al) of chrome spinels is a commonly used parameter to identify the tectonic setting of residual mantle peridotites (e.g., Arai, 1994; Dick & Bullen, 1984; Parkinson & Pearce, 1998), contrasting Cr-numbers of Troodos Mantle Sequence chrome spinel (Batanova & Sobolev, 2000) indicate that the completely serpentinized peridotites of the Artemis domain originate from a region of fertile mantle

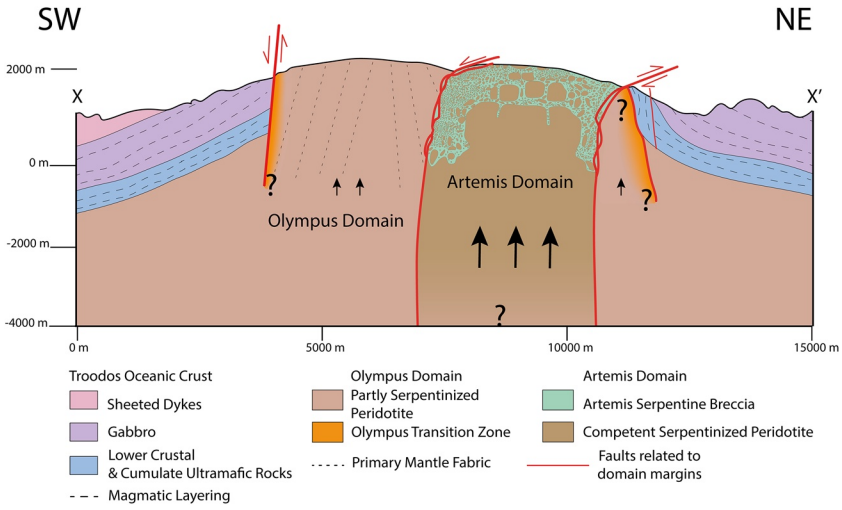

Figure 2. Geological cross-section of the Troodos Mantle Sequence and associated ocean crustal rocks.

lherzolite (Cr# 0.22–0.28) that has been exhumed from depth and juxtaposed against the refractory shallow mantle harzburgites (Cr# 0.51–0.70) of the Olympus domain.

A regional (200 × 100 km^2) oblong positive Bouguer gravity anomaly between +100 and +250 mGal coincides with the Troodos ophiolite (Figure 3a; Gass & Masson-Smith, 1963). This regional positive anomaly generally decreases from west to east across the ophiolite (Figure 3b), with smaller localized anomalies superimposed onto this regional trend (Figure 3a). The variably serpentinized outcrops of the Troodos Mantle Sequence spatially coincide with a large negative gravity anomaly relative to the regional trend (Figure 3a; 80–120 mGal; Gass & Masson-Smith, 1963; Shelton, 1993). This superimposed negative gravity anomaly is broadly centered on the abandoned chrysotile asbestos mine at Pano Amiantos (Figure 1b;

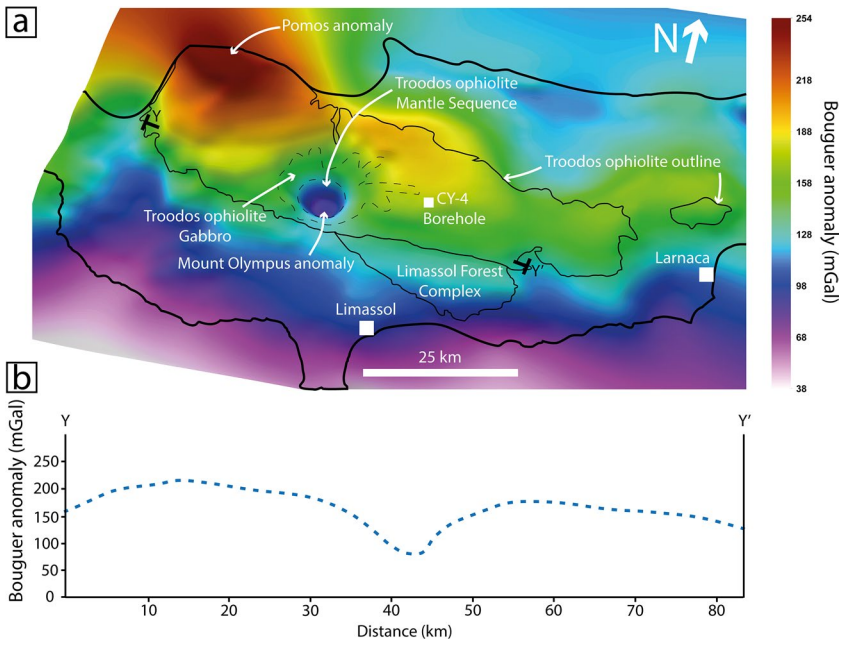

Figure 3. (a) 3D gravity map covering Cyprus, data sourced from Gass and Masson-Smith (1963). (b) Gravity cross-section along line *Y*–*Y*′ again using data of Gass and Masson-Smith (1963), cross-section highlights the asymmetric nature of the Mount Olympus anomaly with the gravity low centered broadly on the former chrysotile asbestos mine of Pano Amiantos.

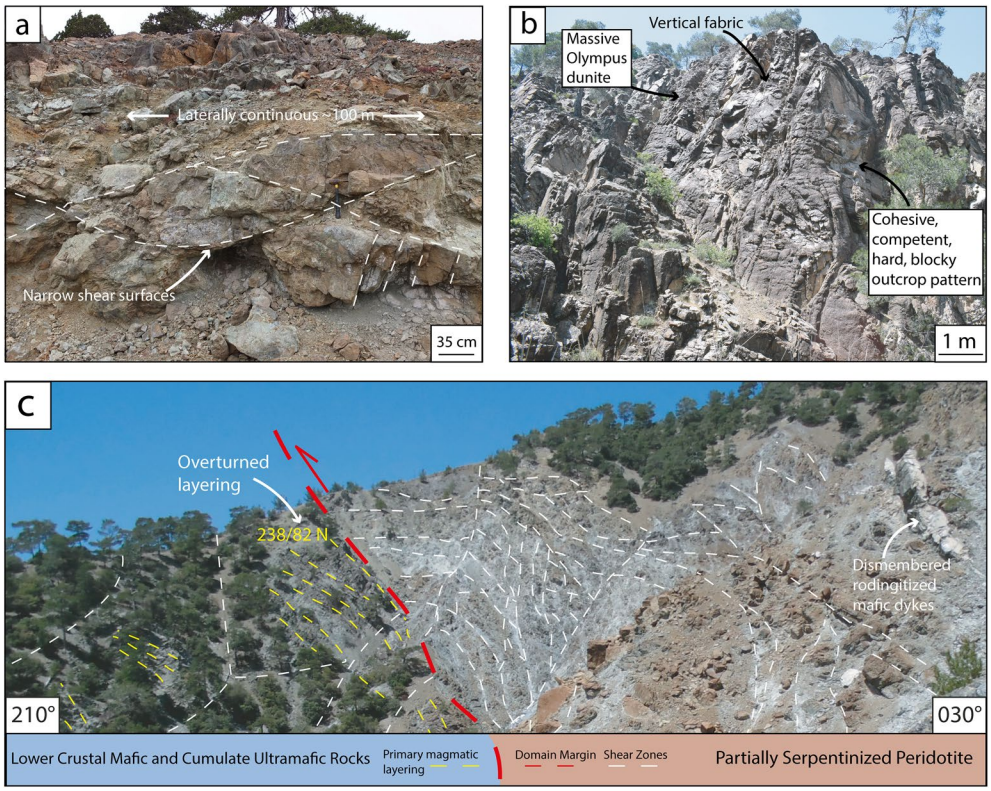

Figure 4. (a) Typical outcrop of partly serpentinized mantle peridotites from the Olympus domain with near horizontal, narrow shear zones orientated 120° apart, that form laterally continuous ~100 m lensoidal geometries. (b) Massive Olympus domain dunite displaying the common hard, blocky, cohesive, partially serpentinized mantle peridotite outcrop pattern. (c) Olympus domain outer boundary highlighting a zone of intensely deformed peridotite and intercalated blocks of overturned layered gabbro.

Gass & Masson-Smith, 1963; Shelton, 1993). In published studies, this negative gravity anomaly is best represented as a vertical, cylindrical body of lower density serpentinized peridotite (2,670 kg/m^3) extending ~11 km deep, within a higher density background of unserpentinized mantle (3,300 kg/m^3; Gass & Masson-Smith, 1963; Shelton, 1993).

3.2. Structure of the Olympus Domain

The rocks of the Olympus domain exhibit a steeply dipping ~NW-SE orientated primary tectonic fabric of elongated orthopyroxene grains, in some places isoclinally folded, that is interpreted as Cretaceous ridge-related high-temperature deformation (Moores & Vine, 1971). Overlaying this primary tectonic foliation are conjugate brittle-plastic shear zones (following Fossen & Cavalcante, 2017; Ramsay, 1980), which in the Olympus domain are thin, localized shear surfaces (~5 cm wide) and laterally continuous for ~100 m (Figure 4a). These shear surfaces intersect and are orientated ~120° to each other (Figure 4a), forming generally undeformed elongated lozenges of partially serpentinized Olympus domain mantle peridotite encompassed by shear surfaces (Figure 4a). Surrounding the summit region of Mount Olympus, conjugate shear zones are orientated at low dip angles and in general progressively steepen away from the summit region to moderate-high dip angles at the margins of the Olympus domain (Figures 1b and 4b). Fracturing at the outcrop scale is minor and manifests as joints and along shear surfaces (Figures 4a and 4b). The Olympus domain displays a distinctive, cohesive, blocky, and competent outcrop pattern (Figure 4b).

There is a complex marginal boundary between the Olympus domain and the encircling plutonic crustal rocks (Figure 4c), which we term here as the Olympus Transition Zone. This zone is of variable width, up to ~1 km at its widest extent, and comprises a generalized transition from predominantly lower ocean crustal cumulate rocks intercalated with localized bodies of dunite and pyroxenite to predominantly mantle rocks

of the Olympus domain, principally harzburgites and dunites with intercalated localized bodies of lower ocean crustal mafic and ultramafic cumulate rocks. Deformation is distributed throughout the Olympus Transition Zone but is mostly localized to an encircling array of steeply dipping interconnected fault-zones that isolate and juxtapose regions of undeformed and massive partially serpentinized bodies with moderately to steeply dipping (60°–>90°) layered gabbros that in places are locally overturned (Figure 4c). This structural style occurs across differing scales from outcrop to hillslope (Figure 1b; see Supporting Information), consequently producing a complex structural unit that anastomoses irregularly around the arcuate periphery of the Olympus domain (Figure 1b). Although on the western slopes of Mount Olympus, some rare, small, fault-isolated regions preserve igneous boundaries between cumulate to mantle rocks, at a larger scale faults always separate the main Olympus domain from the continuous sequences of ultramafic cumulate rocks and gabbros of the lower Troodos ocean crust (Wilson, 1959).

3.3. Structure of the Artemis Domain

To the east of Mount Olympus is the sub-circular Artemis domain that comprises heterogenous assemblages of highly serpentinized blocks and clasts and serpentine gouge, which is juxtaposed by faults against the massive peridotites of the Olympus domain (Figure 5a). The Artemis domain is generally at lower altitude than (>1,200–~1,700 m) the Olympus domain (>1,200–1,952 m) (Figure 5a).

Within the Artemis domain, coherent blocks and clasts (>100 m to dm) are completely serpentinized and occur within a friable matrix of highly comminuted serpentine cataclasite and serpentine clay gouge. In some zones, the serpentine gouges have developed a well-defined secondary foliation fabric (Figure 5b) that anastomoses around the more competent clasts (Figures 5c and 5d). Within the more competent clasts, fibrous asbestiform chrysotile and crack-seal serpentine veining are common on scales from 0.5 mm to ~10 m, forming abundant mutually cross-cutting orthogonal, concentric, and oblique vein sets (Figure 5c). In rare occurrences, serpentine veins cross-cut the Artemis serpentine gouge. Variable proportions and extents of recrystallization occur throughout the Artemis domain (e.g., Figure 5b), with the greatest concentration along localized zones of high strain.

Overall, the Artemis domain comprises an approximately 50:50 mixture of serpentine breccia and gouge to competent serpentinized clasts, although the relative proportions are spatially variable (Figure 5d). The highest proportion of serpentine breccia-gouge to block-clasts is around the subcircular margin of the Artemis domain (~80:20 respectively) with localized regions of 100% recrystallized serpentine gouge (Figure 5b). These areas typically exhibit poorly consolidated steep slopes with active mass wasting and gravity-driven slumping in deeply incised valleys around the periphery of the Artemis domain (Figure 5e).

In contrast, in the central zone of the Artemis domain, the ratio of blocks-clasts to serpentine breccia-gouge is reversed, with large (>100 m) blocks of strongly altered peridotite separated by complex networks of relatively narrow (~10 m) serpentine breccia (Figure 2).

4. Contrasting Properties Within the Troodos Mantle Sequence

4.1. Contrasting Mineralogy

The serpentinization style within the Olympus domain reflects the partial transformation (~50%–~70%) of primary olivine and orthopyroxene to serpentine through serpentinization hydration reactions (Figure 6a, Table 1). In contrast, the completely serpentinized materials of the Artemis domain reflect multiple and potentially on-going episodes of deformation, alteration, and recrystallization (Figure 6b). Primary and alteration bulk assemblages are estimated from thin section and outcrop observations. Distinguishing between different serpentine polymorphs is challenging (Rooney et al., 2018, and references therein) so consequently we describe them all simply as serpentine, except for fibrous chrysotile and rare occurrences of "splintery" antigorite.

The rocks of the Olympus domain are predominantly tectonized harzburgites originally composed of olivine, orthopyroxene, chromite, and minor interstitial diopside, with subsidiary dunites, and some primary orthopyroxene veins. These rocks are partially to completely altered to olivine-serpentine mesh-textures

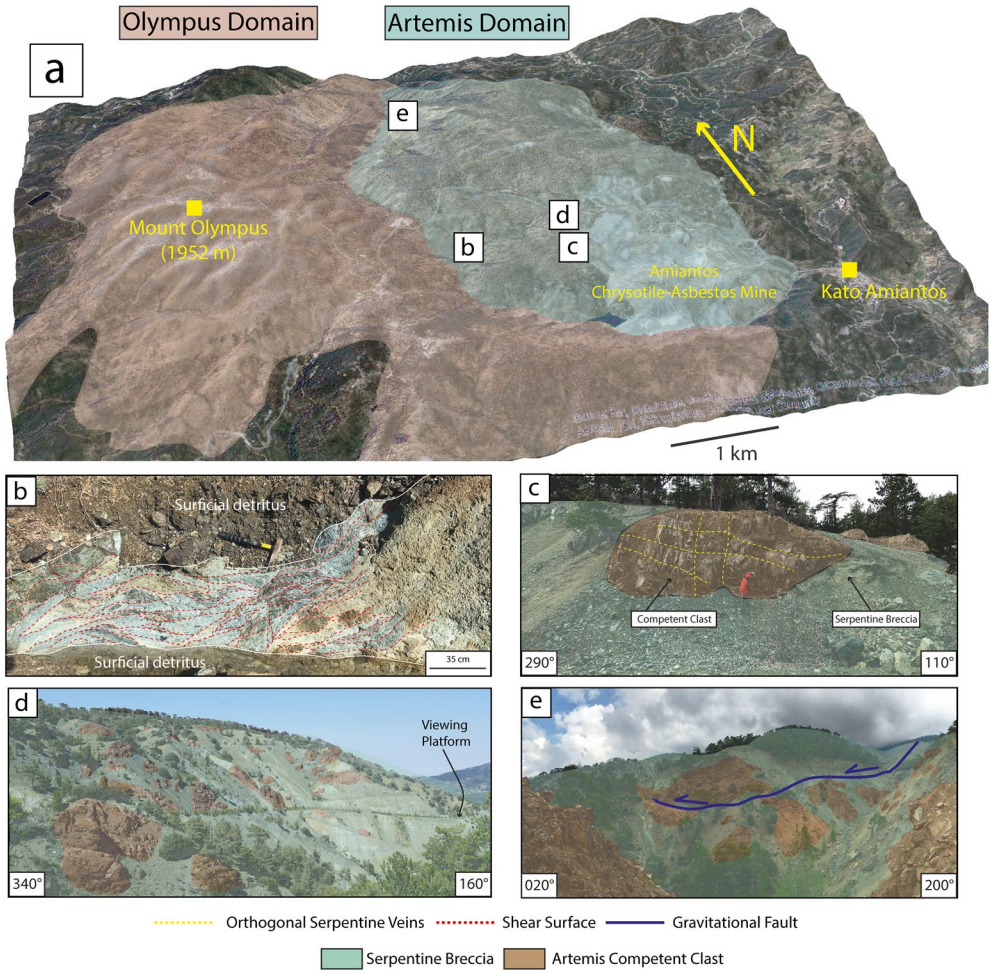

Figure 5. (a) 3D satellite-terrain hybrid image of the Troodos Mantle Sequence, highlighting the extent and differences in terrain and geomorphology between the Olympus and Artemis domains. Locations of inset images (b)–(e) shown. (b) Artemis domain serpentine gouge displaying the complex and intricate structure within recrystallized serpentine breccia-gouge. Hammer for scale. (c) Competent serpentinite block-clast with mutually cross-cutting orthogonally orientated serpentine veins, that is surrounded by highly comminuted serpentine cataclasite and localized serpentine gouge. (d) Artemis domain clast-gouge mountainside structure, highlighting the complex domain-wide network of isolated competent serpentinized block-clasts surrounded by weaker serpentine breccia-gouge. Viewing platform overlooking the former Amiantos asbestos mine for scale. (e) Actively collapsing Artemis domain hillslopes due to high proportions of weak, friable, and serpentine gouge.

and some magnetite, with trace dolomite and calcite, and minor ~1-mm-wide serpentine veins (Figure 6a). Serpentine-filled microfractures are abundant at the micron scale (Figure 6a).

In contrast, the competent clasts of the Artemis domain are composed of mixed serpentine and chrysotile, including the complete bastitic replacement of primary orthopyroxene. Serpentine, predominantly fibrous chrysotile, occurs as discrete mutually cross-cutting extensional and hybrid crack-seal veins. The breccia matrixes and gouges comprise serpentine variably recrystallized to different grain sizes (Figure 6b). Multiple episodes of serpentinization, deformation, dissolution, and recrystallization are likely reflected in the breccia matrixes and gouges. In rare occurrences antigorite forms as discrete veins (e.g., Magaritz & Taylor, 1974) and as brecciated clasts (0.1–2 mm) surrounded by recrystallized serpentine. Chromite is the only primary mantle phase preserved in the Artemis domain rocks. Globular hydro-andradite occurs throughout the blocks within the Artemis domain, and also forms as discrete veins associated with serpentine veins. Calcite occurs as discrete late-stage veins generally cross-cutting serpentine veins.

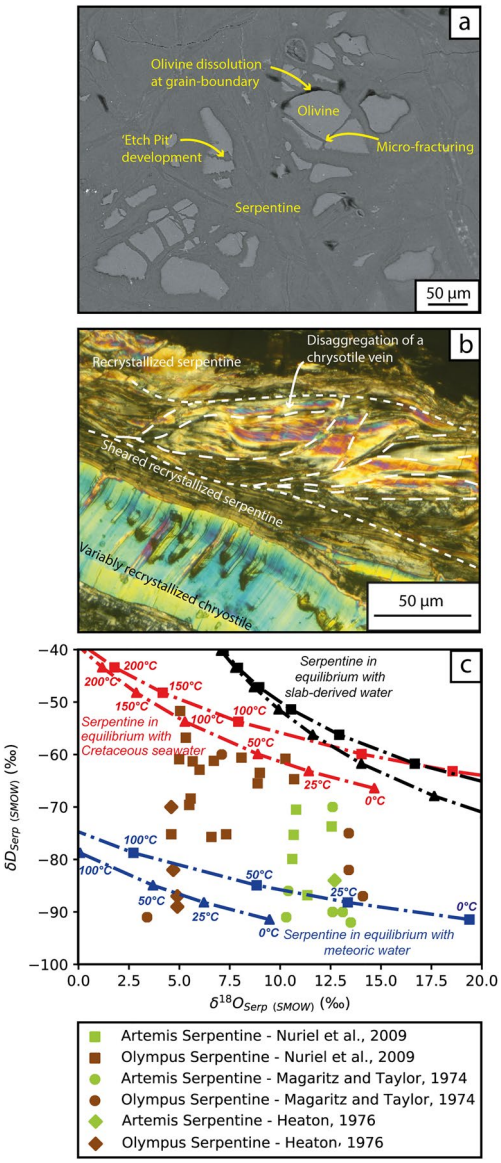

Figure 6. (a) Scanning electron microscope back-scattered electron (BSE) image of the partly serpentinized Olympus domain with the olivine-serpentine mesh interface highlighted. Common micro-fracturing associated with the dissolution and transformation of primary olivine to secondary serpentine through the serpentinization style of partial serpentinization hydration reactions. (b) Cross-polarized light photomicrograph of a typical Artemis domain completely serpentinized competent clast with variable dynamically recrystallized serpentine and associated cataclastic deformation. (c) Oxygen and hydrogen stable isotope plot of published serpentine measurements (Heaton, 1976; Magaritz & Taylor, 1974; Nuriel et al., 2009). Troodos Mantle Sequence values are separated based on sample location either from the Olympus or Artemis domain. Calculated serpentine oxygen and hydrogen stable isotope values in equilibrium with Cyprus meteoric water (δ^{18}O −7‰, δD −35‰; e.g., Boronina et al., 2005), Cretaceous seawater (δ^{18}O −1‰, δD −7‰; e.g., Heaton & Sheppard, 1977), and slab-derived metamorphic water (δ^{18}O +7.8‰, δD −15‰; e.g., Alt & Shanks, 2006) are shown. Triangles represent calculated serpentine values in equilibrium using empirical oxygen isotope fractionation factors from Wenner & Taylor, 1971 and hydrogen isotope fractionation factors from Saccocia et al. (2009). Squares represent calculated serpentine values in equilibrium using semi-empirical oxygen isotope fractionation factors from Zheng (1993) and empirical hydrogen isotope fractionation factors from Saccocia et al. (2009).

Table 1
Contrasting Characteristics, Properties and Serpentinization Styles Exhibited by the Proposed Olympus and Artemis Domains of the Troodos Mantle Sequence

	Olympus domain	Artemis domain
Serpentinization degree	~50%–70%	100%
Serpentinization style	Hydration of primary igneous mineralogy	Coupled serpentine deformation-alteration-recrystallization
Fabric	Primary—tectonitized localized serpentinized shears, cm to decimeter wide	Extensive secondary, polyphase shears, weak and soft serpentine breccia with component serpentinized clasts 1 cm to >100 m
Fractures	Minor fracturing	Extensive on all scales from micron to ~100 m
Chrysotile and serpentine veins	None, minor, ~2 mm wide serpentine veins uncommonly occur around domain periphery	Abundant orthogonal, concentric, oblique on all scales from sub-mm to 20 cm
Shear zones	Laterally continuous up to 100 m, narrow <1 m, discrete, localized shear surfaces orientated 120° apart	Pervasive, dominating entire body from mm to >1 km, anastomosing/surrounding competent, rigid clasts
Competence	Cohesive, hard, blocky	Friable, incohesive
Density	2,686 ± 83 kg/m^3	1,949 ± 47 kg/m^3
Ground water	Low to very low, few perennial streams, ephemeral streams and seeps, no springs	Moderate to high, numerous ephemeral seeps and springs, several moderate-large perennial streams
Topographic expression	Mt. Olympus high point	Collapsing slopes, valleys
Erosion rate	Low, vegetated slopes, steep, large, rocky outcrops, narrow gorges	High, actively collapsing, vegetation-free steep slopes – angle of repose >30°
Inferred uplift initiation age	~5.5 Ma	<1 Ma?
Oxygen and hydrogen stable isotope values	δ^{18}O +7.1 ± 3‰ (1σ)	δ^{18}O +11.8 ± 1.2‰ (1σ)
	δD −70.3 ± 10.8 ‰ (1σ)	δD −82.4 ± 8.2‰ (1σ)

4.2. Contrasting Serpentine Oxygen and Hydrogen Stable Isotope Values

Published serpentine oxygen and hydrogen stable isotope values (e.g., Heaton, 1976; Magaritz & Taylor, 1974; Nuriel et al., 2009) differ for the Olympus domain and the Artemis domain (Figure 6c; Table 1). The Artemis domain values exhibit a shift to higher oxygen stable isotope values relative to the Olympus domain (Figure 6c; e.g., Heaton, 1976; Magaritz & Taylor, 1974; Nuriel et al., 2009). Calculated serpentine oxygen and hydrogen stable isotope values in equilibrium with meteoric water (δ^{18}O −7‰, δD −35‰; e.g., Boronina et al., 2005) at temperatures >25°C to <100°C and Cretaceous seawater (δ^{18}O −1‰, δD −7‰; e.g., Heaton & Sheppard, 1977) at temperatures <150°C fall into the respective outer limits of the Olympus domain values (Figure 6c). In contrast, serpentine oxygen and hydrogen stable isotope values of the Artemis domain fall into a narrower range (δ^{18}O +10.3‰ to +13.5‰; δD −70‰ to −92‰) compared to the Olympus domain (δ^{18}O +3.4‰ to +14.1‰; δD −52‰ to −92‰; Figure 6c; Heaton, 1976; Magaritz & Taylor, 1974; Nuriel et al., 2009). There is greater range in the Artemis domain hydrogen stable isotope values compared to oxygen stable isotope values (Figure 6c). Calculated serpentine oxygen isotope values in equilibrium with meteoric water (δ^{18}O −7‰, δD −35‰; e.g., Boronina et al., 2005) at temperatures ~25°C–~50°C fall within the measured range of Artemis domain oxygen isotope values (Figure 6c). However, only some of the measured Artemis domain hydrogen stable isotope values match the equivalent equilibrium calculations (Figure 6c). The calculated serpentine oxygen and hydrogen stable isotope values in equilibrium with a slab-derived serpentinizing fluid (δ^{18}O +7.8‰, δD −15‰; e.g., Alt & Shanks, 2006) do not match any previously measured oxygen and hydrogen stable isotope values (Figure 6c).

4.3. Contrasting Bulk Densities

Bulk dry densities were measured on mini-cores taken from selected representative samples from the Troodos ophiolite Mantle Sequence including samples from each of the Olympus and Artemis domains (Table 2). The bulk density of the partly serpentinized peridotites of the Olympus domain is 2,686 ± 83 kg/m^3 (1σ,

Table 2
New Density Measurements With Estimated Primary and Secondary Modal Mineral Assemblages

Sample	Sample type	Density (kg/m^3)	Primary mineralogy assemblage (%)	Secondary Mineralogy Assemblage (%)
AH2	Olympus Dunite	2,760	30–50	50–70
AH1	Olympus Harzburgite	2,797	30–50	50–70
AJ2H	Olympus Harzburgite	2,565	30–50	50–70
AJ2V	Olympus Harzburgite	2,565	30–50	50–70
PP3-20	Olympus Harzburgite	2,699	30–50	50–70
PP3-16	Olympus Harzburgite	2,706	30–50	50–70
PP2-11	Olympus Dunite	2,708	30–50	50–70
PP2-15	Olympus Dunite	2,688	30–50	50–70
AR2	Artemis Clast	2,292	0	100
AR1	Artemis Clast	2,294	0	100
PP1-23	Artemis Clast	2,390	0	100
PP1-22	Artemis Clast	2,268	0	100
PP1-25	Artemis Clast	2,408	0	100
BZ1	Artemis Breccia	1,545	0	100
BZ2	Artemis Breccia	1,505	0	100
DC1V	Artemis Breccia	1,559	0	100
DC2H	Artemis Breccia	1,502	0	100
DH1V	Artemis Breccia	1,607	0	100
DH2H	Artemis Breccia	1,691	0	100
DSDP Leg 37 ($n = 5$)*	Serpentinized peridotite	2,699		
Mantle**	Unserpentinized Mantle	3,300	100	0

Sample Type	Average Density (kg/m^3)	1σ	Competent Clast (%)	Serpentine Breccia (%)
Olympus	2,686	86		
Artemis Clast	2,330	63 (δa)	100	0
Artemis Breccia	1,568	71 (δb)	0	100

Sample type	Average Density (kg/m^3)	([a]) Propagated Error (δz)	Competent Clast proportion (x)	Serpentine Breccia proportion (y)
Artemis Breccia	1,949	47	0.5	0.5
	1,759	56	0.25	0.75
	2,139	51	0.75	0.25
	2,177	51	0.8	0.2
	1,720	58	0.2	0.8
	1,873	50	0.4	0.6
	2,025	47	0.6	0.4

Note. DSDP Leg 37 average density of serpentinized peridotite from Hyndman and Drury (1976). Average density of unserpentinized mantle peridotite from Birch (1961). Calculated errors for differing proportions of Artemis clast and gouge are also shown.

*Hyndman and Drury (1976).

**Unserpentinized mantle peridotite (Birch, 1961).

[a] $\delta z = \sqrt{\left(x \times \delta a\right)^2 + \left(y \times \delta b\right)^2}$

$n = 8$). In contrast, the serpentinized clasts from the Artemis Domain have bulk densities of 2,330 ± 63 kg/m^3 (1σ, $n = 5$) and the serpentine breccias yield very low densities of 1,568 ± 71 kg/m^3 (1σ, $n = 6$; Table 2, Figure 4b). Given the approximately 50:50 mix of clasts to breccia across the whole Artemis domain, we estimate a gross bulk density of ~1,949 ± 47 kg/m^3 (Table 2). Background unserpentinized mantle peridotite has an inherit bulk density of 3,300 kg/m^3 (Birch, 1964; Gass & Masson-Smith, 1963).

5. Constraints on the Timing of the Uplift and Exposure of the Troodos Ophiolite

The Troodos ocean crust is relatively thin, only ~4,000 m thick from the top of the extrusive rocks to the uppermost mantle peridotites (Malpas, 1989). However, this still requires that a minimum of ~4,000 m of exhumation must have occurred since the initial subaerial emergence of the Troodos ophiolite. The circum-Troodos sediments in the Mesaoria and Pissouri basins surrounding the Troodos Ophiolite (Figure 1a) preserve stratigraphic records of the unroofing and erosion of progressively deeper levels of the Troodos ophiolite (McCallum, 1989; Poole & Robertson, 1991, 1998; Robertson, 1977; Rouchy et al., 2001; Stow et al., 1995; see supporting information). Significant amounts of Troodos-derived diabase and lava clasts occur in the latest Messinian/Early Pliocene (~5.5 Ma) strata indicating significant subaerial relief and exposure of the uppermost Troodos crust by this time (McCallum, 1989; Rouchy et al., 2001; Stow et al., 1995). Gabbroic clasts are first recorded in the Late Pliocene (McCallum, 1989; Stow et al., 1995). The proportion of gabbroic clasts is significantly greater in the Pleistocene Fanglomerates than the Pliocene successions (McCallum, 1989; Poole & Robertson, 1991, 1998). The first occurrence of ultramafic clasts is recorded within the Lower Pleistocene (<2.58 Ma) sequence (Poole & Robertson, 1991, 1998; Stow et al., 1995; Wilson, 1959). The abundance of ultramafic clasts progressively increases within the Pleistocene Fanglomerate sequences (2.58–0.0117 Ma) (Poole & Robertson, 1991, 1998). The Plio-Pleistocene sedimentary sequences have been interpreted to record pulses of uplift focused on Mount Olympus (e.g., McCallum, 1989; Poole & Robertson, 1991, 1998; Robertson, 1977), with the intensity of the uplift episodes having waned from the Late Pleistocene to the present day (Poole & Robertson, 1998).

Low-temperature (U-Th)/He thermochronology on plutonic rocks from the Troodos Massif suggests an exhumation rate of 0.86 mm/yr with the onset of uplift at 6 ± 2 Ma (Morag et al., 2016). This rate broadly agrees with the uplift trajectory compiled from clast occurrences in the circum-Troodos sedimentary sequences (McCallum, 1989; Poole & Robertson, 1991, 1998; Rouchy et al., 2001; Stow et al., 1995).

6. Mechanistic Uplift Modeling

Explanation of the formation of the unique geometry of the Troodos Massif must address a number of key observations: (a) Uplift must occur within the well-constrained uplift trajectories from circum-Troodos sedimentary sequences (e.g., Follows, 1990; McCallum, 1989; Poole & Robertson, 1998; Robertson, 1977, 1998; Stow et al., 1995) and recent thermochronology (Morag et al., 2016); (b) Invoke a mechanism that explains the differential uplift between the exhumed Troodos Mantle Sequence atop Mount Olympus and the regionally uplifted mantle peridotites that underlie the remaining ocean crustal sequences; (c) Account for the subdivision of the Troodos Mantle Sequence into two distinct domains and their respective contrasting properties that has induced further uplift and exhumation of the Artemis domain relative to the Olympus domain. Here, we develop a one-dimensional uplift model for the Troodos Mantle Sequence to determine whether it is mechanistically possible to generate the observed ~2,000 m relief through a density contrast-driven isostatic response since ~5.5 Ma, whilst parameterizing for the subdivision of the Troodos Mantle Sequence.

6.1. Model Parameters

Using reasonable parameters for the Troodos ophiolite (Table 3), elevation is determined in a number of iterative steps by subtracting erosion from the isostatic uplift generated by an advancing one-dimension serpentinization front within a period of time, from an initial elevation of 0 m (Equation 1, Figure 7a, Table 3).

$$\text{Elevation} = \text{Uplift} - \text{Erosion} \quad (1)$$

Table 3
Model Parameters for the Olympus and Artemis Domains Used in the Mechanistical Uplift Modeling

Symbol	Definition	Olympus domain parameters	Artemis domain parameters	Unit
S_D	Serpentinization front distance			m
S_r	Serpentinization front rate	(200, 1,000, 2,000, 3,000)	(600, 3,000, 6,000, 9,000)	m/Myr
H	Time period			Myr
	Time steps	10,000	2,000	
φ_D	Stretching distance			m
B	Stretching percentage	20% = 50% Serpentinization	40% = 100% Serpentinization	
D_D	Domain thickness/depth			m
U_t	Total uplift from isostatic response			m
ρ_M	Density of residual material	3,300 (background lithospheric mantle)	2,700 (Olympus)	kg/m^3
ρ_D	Domain density	2,700 (Olympus)	2,000 (Artemis)	kg/m^3
E_r	Erosion rate			m/Myr
ε_t	Erosion response time			Myr
τ_e	Bedrock erodibility coefficient	1.5×10^{-6}	6.4×10^{-6}	m
ω	Precipitation	910	910	mm/yr
E	Erosion			m

The serpentinizing front advances at an estimated average rate (S_r) for a given time period (η). This generates a depth (S_D) for the serpentinization front (Equation 2, Figure 7a).

$$S_D = S_r \times \eta \tag{2}$$

We assume that the advancing serpentinizing front occurs within a horizontally confined structure, advancing into background unserpentinized peridotite with a density of 3,300 kg/m^3. Serpentinization reactions reduce density and result in volume expansion. Assuming that the horizontally confined structure expands (Equation 3) in the vertical direction, the total percentage of volume expansion (β) is related to the total average serpentinization percentage above the advancing front. The rocks of the Olympus Domain are on average approximately ~50% serpentinized, and this produces a ~20% volume expansion (100% serpentinization results in ~40% bulk volume expansion).

$$\varphi_D = \left(\frac{S_D}{100}\right) \times \beta \tag{3}$$

The total depth of the expanded advanced serpentinizing front (φ_D) in a given time period added to the serpentinization front depth (S_D), yields the total depth (D_D) (Equation 4)

$$D_D = S_D + \varphi_D \tag{4}$$

D_D is then input into an isostatic calculation to determine the isostatic change in elevation over an increment of time, to the density difference between background ultramafic unserpentinized mantle (ρ_M) and a horizontally confined, vertical serpentinized body (ρ_D). The uplift due to isostatic response (U_t) of an advancing serpentinization front is equal to the total uplift (Equation 5) (Figure 7a).

$$U_t = \left(\frac{\rho_M - \rho_D}{\rho_M}\right) \times D_D \tag{5}$$

We then apply an erosional model (following e.g., Cao & Paterson, 2016; Lee et al., 2015; Simoes et al., 2010) to calculate the erosion rate (E_r) for a time period (Equation 6).

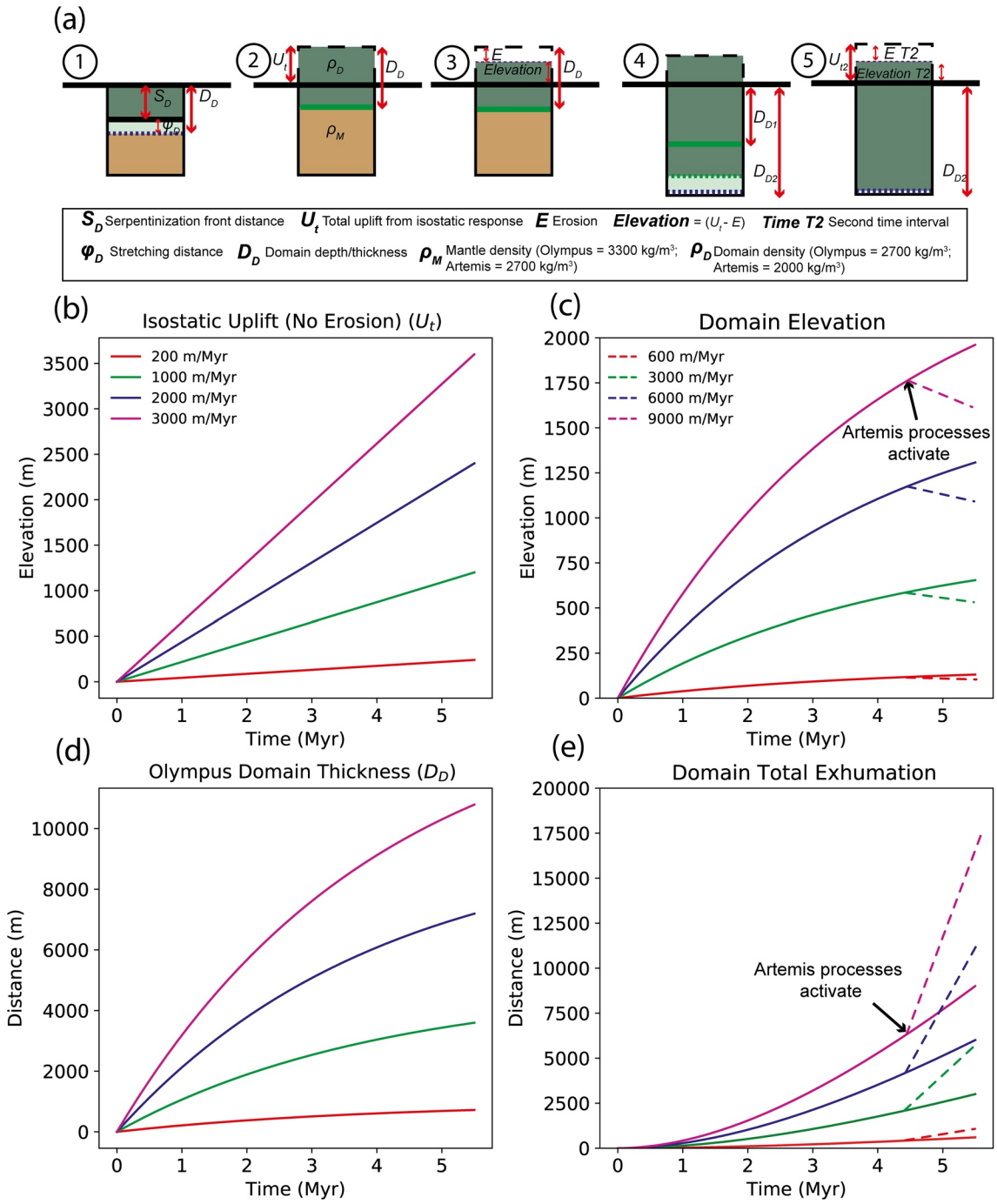

Figure 7. (a) Uplift model set up. One-dimensional horizontally confined model where elevation is determined by subtracting erosion from the isostatic uplift in response to an advancing average serpentinization transformation front. Model is repeated over a number of iterative steps from an initial elevation of 0 m for a total run time of 5.5 Myr. Differing parameters are utilized for each domain (see Table 3). (b) Olympus domain isostatic uplift output shown with no erosion applied. Output highlights the theoretical maximum surface uplift that can be generated through an advancing average serpentinization transformation front. (c) Olympus domain elevation model output shown, where differential erosional parameters are applied to the uplift model, generating an elevation value through subtracting erosion from surface uplift. Artemis domain total elevation output is also shown in dashed. Inflection point at 4.4 Myr highlights the change in parameterization from Olympus to Artemis (Table. 3). (d) Olympus domain evolving thickness output shown highlights the interplay between erosion and the advancing serpentinization front in producing the thickness of the domain. (e) Olympus domain exhumation total is shown along with the Artemis domain exhumation total (in dashed). Inflection point at 4.4 Myr represents the activation of Artemis parameters (see Table 3).

$$E_r = \frac{U_t}{\varepsilon_t} \tag{6}$$

$$\varepsilon_t = \frac{1}{\tau_e \times \omega} \tag{7}$$

$$E = E_r \times \eta \tag{8}$$

The erosion rate (E_r) is a function of the isostatic response uplift (U_t) and erosion response time (ε_t). The erosional response time is a function of the bedrock erodibility constant (τ_e) and average annual precipitation (ω) (Equation 7). By multiplying the erosion rate with the time period (η), the total erosion (E) for that time period can be calculated (Equation 8). Each step is repeated 10,000 times over a defined time period of 5.5 Myr.

6.1.1. Advancing Serpentinization Front Rates

A range of one-dimensional average advancing serpentinization front (S_r) rates are input into the Olympus mechanistical uplift model (Table 3) to determine the contribution of an advancing serpentinization front to uplift and unroofing of the Troodos Massif mantle peridotites. The range of Olympus domain one-dimensional serpentinization front advancement rates (S_r; 200–3,000 m/Myr) used in our model are broadly equivalent to serpentinization rates proposed with other serpentinization studies in seafloor settings (e.g., Lowell & Rona, 2002) and experimentally determined one-dimensional serpentinization hydration reaction "diffusion" rates that range between ~200 m/Myr and ~4,000 m/Myr (e.g., Lamadrid et al., 2017; Macdonald & Fyfe, 1985; Martin & Fyfe, 1970; McCollom et al., 2016). However, the rate of our advancing one-dimensional serpentinization front (S_r) is not strictly equivalent to an experimentally determined serpentinization diffusion rate because our simple uplift model does not explicitly consider fluid channeling or the spacing of cracks and channels.

In contrast, the Artemis domain does not express a simple progressive hydration/serpentinization style but coupled near-surficial to surficial deformation-alteration-recrystallization serpentinization processes. Surficial to near-surficial serpentinization rates are interpreted to be geologically rapid (e.g., Craw et al., 1987). Modeling of the interplay between chrysotile dissolution-recrystallization rates (e.g., Thom et al., 2013) and grain size in differing surficial (22°C), fluid-saturated pH conditions indicates that pH 8 a ~1 mm chrysotile particle would dissolve and recrystallize in ~20,000 years, whereas under the same conditions a ~1-m-sized particle size would take ~20 Ma (see supporting information). Consequently due to grain size reductions, coupled deformation-alteration-recrystallization mechanisms at surficial conditions within the Artemis domain are likely to occur at faster reaction rates than the hydration serpentinization style of the Olympus domain. This reflects the contrasting structural characteristics of each domain (Figure 5c) and is likely to continue to some degree at depth due to greater fracture density within the Artemis domain relative to the Olympus domain. To reflect this within the Artemis uplift model, the Artemis advancing transformation rate (S_r) is tripled relative to the Olympus domain.

6.1.2. Uplift Model Assumptions and Limitations

It is assumed that the isostatically uplifted Troodos ocean crust had a similar density and bedrock erodibility constant (τ_e) to partially serpentinized peridotites (2,700 kg/m^3). It is assumed that there is no "lag" time between the advance of the serpentinizing front and isostatic uplift. Within the model set-up, we assume a horizontally bound vertical structure, where the advancing serpentinization front and associated volume expansion occur only in the vertical direction. Although it is easier to conceptualize the model with fluid infiltration from the surface, the model is not reliant on whether the serpentinization fluid source is from above, below, or a combination of both since the mass-change outcome is the same in our one-dimensional setup. We assume that the advanced serpentinization front depth (S_D) is an average serpentinization percentage for the whole vertical structure. The model does not account for gravitational collapse. Nor does it account for thermo-mechanical boundary effects between the serpentinized portion and background unserpentinized mantle during exhumation/uplift. It is assumed that present-day precipitation levels of

910 mm/yr (Prodromos village, 1,400 m asl, Cyprus Department of Meteorology) are representative of rainfall throughout the model time frame. This may be an over-estimation as precipitation generally increases with elevation, and hence may have been lower during the initial stages of uplift. Although during the Plio-Pleistocene periods of greater humidity and precipitation levels than the present-day have been inferred from the relative abundance of sapropels (e.g., Poole & Robertson, 1998 and references therein). We propose a 1.1 Ma date (Mid Pleistocene) for the initiation of the Artemis domain alteration and deformation processes that must start some time between the initial exhumation and protrusion of ultramafic rocks in the Early Pleistocene and the end of the Pleistocene.

6.2. Uplift Modeling Results

6.2.1. Olympus Domain

A serpentinization transformation front advancing at a rate of 3,000 m/Myr will isostatically uplift rock a total of 3,600 m in 5.5 Myr, for a density contrast of 600 kg/m^3 (Figure 7b). Applying reasonable erosional parameters of 910 mm/yr precipitation and a bedrock erodibility of 1.5×10^{-6} m to the same uplift parameters (S_r = 3,000 m/Myr, $\Delta\rho$ = 600 kg/m^3) yields an elevation of ~1,950 m for the Olympus domain after 5.5 Myr (Figure 7c). Under the same model conditions, adjustment of the bedrock erodibility parameter from 1.5×10^{-6} m to 1×10^{-6} m and 2×10^{-6} m produces elevation values of ~2,350 and ~1,650 m respectively. Calculations of the evolving eroded total thickness (Figure 7d) and the total exhumation (Figure 7e) of the Olympus domain for different average advancing serpentinization front rates (S_r), suggests that up to ~9,000 m of material has been exhumed from the Olympus domain over 5.5 Myr.

6.2.2. Artemis Domain

To quantify the dynamic topography resulting from a secondary density contrast between the Artemis (2,000 kg/m^3) and Olympus (2,700 kg/m^3) domains, the elevation model is re-run using the Artemis model parameters (Table 3). After 4.4 Myr of the 5.5 Myr run time, the Artemis domain overprints the Olympus domain, generating a joint contribution to the uplift and differential exhumation of the Artemis domain. The advancing serpentinization front rate (S_r) of the Artemis domain is tripled. The bedrock erodibility constant (τ_e) is also increased to 6.4×10^{-6} m to account for the weak, friable, easily erodible material. Calculations using these parameters yield a lower elevation (~1,550 m) for the Artemis domain compared to the Olympus domain peak (1,952 m) (Figure 7c), in line with the current present elevations. Using the parameters applied, modeling suggests that ~17.5 km of material has been exhumed over 5.5 Myr period (Figure 7e and Table 3).

7. Discussion

7.1. Serpentinite Diapirism of Troodos Mantle Sequence

New measurements of the bulk densities of the Olympus and Artemis domains, and simple modeling indicate that mountains akin to Mount Olympus (~2,000 m elevation asl) can form within the required time constraints (~5.5 Myr; see supporting information) solely through serpentinization with the resultant density contrast causing isostatic uplift. Serpentinization alone is therefore mechanistically capable of producing the progressive uplift and exhumation that has culminated in the solitary, relatively high-altitude peak (1,952 m) of Mount Olympus, relative to the low to modest altitude of the sheeted dike complex (~1,000 m). We interpret the Olympus domain as a distinct serpentinite diapir that has resulted in the transportation and protrusion of mantle peridotites to 1,952 m asl above the regionally uplifted mantle peridotites that underlie the ophiolitic ocean crust. The minimum differential uplift of the Olympus diapir compared to the regionally uplifted "in-situ" Troodos ophiolite mantle peridotites can be estimated by considering the Cyprus Crustal Study Project CY-4 drill hole located near the village of Palaichori (~930 m asl) ~20 km east of Mount Olympus. With a total depth beneath the surface of 2,263 m, CY-4 penetrated sheeted dikes, gabbro, and lower crustal ultramafic cumulate rocks but did not reach tectonized upper mantle peridotites (Malpas et al., 1989). Assuming that the CY-4 drill hole would have intersected mantle peridotites at a depth of 2,500 m beneath the surface (1,600 m below sea level) the minimum required relative uplift is ~3,600 m.

We interpret the Artemis domain as a second, overprinting and distinct serpentinite diapir that has cannibalized the eastern portion of the Olympus diapir through coupled deformation-alteration-recrystallization processes to form a 100% serpentinized region (~1,949 ± 47 kg/m^3) with a large proportion of low-density breccia (1,568 ± 71 kg/m^3). Although the lower density of the Artemis diapir results in a greater amount of total isostatic uplift, its weak and easily erodible nature results in differential exhumation between both domains and a lower average elevation of the Artemis diapir (~1,550 m) compared to the Olympus diapir (>1,500–1,952 m).

Differences between the properties and characteristics of both diapiric boundaries, serpentinization extents, alteration mineralogy, deformation styles, geomorphology, density, and outcrop patterns indicate that the Artemis domain overprints and builds on pre-existing Olympus diapir serpentinization and uplift (Figure 2). This culminates in a distinct coupled serpentine deformation-alteration-recrystallization serpentinization style that is in direct contrast to the partial hydration serpentinization style of the Olympus diapir.

The initial localization of greater extents of serpentinization in the Artemis diapir must result from structural controls that have been obscured by on-going deformation as the Artemis diapir expands into the Olympus diapir. The high altitude of the Troodos Mountains and associated rainfall combined with strongly deformed rocks has enabled the incursion of meteoric fluids into the rocks results in increased serpentinization of the uplifted peridotites. An inevitable consequence of meteoric water incursion and serpentinization is the augmentation of a localized deformation-alteration-recrystallization positive-feedback mechanism that initiated the development of the overprinting Artemis diapir. These mechanisms induce the formation of the easily erodible rock, and consequently result in further uplift and exhumation relative to the Olympus diapir. By applying reasonable parameters to the uplift model, the total exhumation of the Artemis diapir is calculated to range between >3.6 and ~17.5 km (Figure 7e). Testing will require further detailed petrological and thermodynamic investigations.

There are clear geochemical differences between the rocks of the Olympus diapir and Artemis diapir. Previous oxygen and hydrogen stable isotope measurements (e.g., Heaton, 1976; Magaritz & Taylor, 1974; Nuriel et al., 2009) yield different measured values for the Olympus and Artemis diapirs (Figure 6c). Calculated oxygen and hydrogen serpentine stable isotope values in equilibrium with meteoric water at varying temperatures (Figure 6c) indicate that the Artemis diapir and portions of the Olympus diapir serpentinites equilibrated with low-temperature (~25°C–<100°C) meteoric water at or near the surface since the unroofing of mantle peridotites during the Early Pleistocene (Poole & Robertson, 1998; Wilson, 1959), and these reactions and exchanges are probably on-going. Serpentine hydrogen stable isotopes have been proposed to exchange with subsequent fluid episodes, potentially overprinting original values (e.g., Kyser & Kerrich, 1991; Kyser et al., 1999; Wenner, 1971). Since the proportions in the balance between oxygen and hydrogen in the fluid and rock are different, hydrogen is more likely to undergo post-formational isotopic exchange relative to oxygen; serpentine oxygen stable isotope values are likely to be more robust. The high δ^{18}O values of the Artemis diapir and portions of the Olympus diapir (δ^{18}O +10.3‰ to +14.1‰) suggest formation at low temperatures, likely with meteoric water (Figure 6c). Regardless of whether or not these values have been overprinted, they highlight that discreet portions of the Olympus and Artemis diapirs have likely interacted and exchanged with differing fluids. Our 1-D models are not sensitive to where fluid ingress and serpentinization occur and are consistent with a component of the uplift resulting from the focused upwelling into the overlying mantle wedge of hydrous fluids generated by the dewatering of partially subducted marine sediments and ocean lithosphere beneath the Troodos rocks, as has been proposed to have initially serpentinized the Troodos Mantle Sequence, inducing serpentinite diapirism (Gass, 1977; Moores & Vine, 1971; Robertson, 1977, 1998). Although there is strong evidence for two distinct textural and geochemical mantle domains (Batanova & Sobolev, 2000), direct evidence for the initial serpentinizing fluid remains elusive. Further geochemical and isotopic investigations are required to better constrain the sequence of fluid-rock exchanges that have occurred during the progressive serpentinization of the Troodos Mantle Sequence.

7.2. Previous Uplift Mechanisms Attributed to the Troodos Mantle Sequence

Previous studies, either do not or only partially satisfy the key criteria outlined in Section 6 necessary to explain the geometry of the Troodos Massif. Although there is compelling evidence in the Limassol

Forest Complex for the Cretaceous seafloor exhumation of mantle rocks (e.g., MacLeod, 1988, 1990; Murton, 1986), geological evidence for similar exposure of the Troodos Massif mantle rocks is less forthcoming. Models that suggest the preservation of Cretaceous seafloor ridge-related detachment faulting (e.g., Nuriel et al., 2009) and Cretaceous ridge-related serpentinite diapirism (e.g., Schuiling et al., 2011) are incompatible with uplift trajectories. These models propose that the exhumation of the Troodos ultramafic rocks occurred on the Cretaceous seafloor. This would require the preservation of original Cretaceous sea-floor relief through its progressive uplift from ocean depths to the current high elevation 1,952 m massif, but would also result in an inverted circum-Troodos sedimentary sequence, with the initial sequences rich in ultramafic materials as opposed to the basalts and diabase observed (Follows, 1990; McCallum et al., 1989; Rouchy et al., 2001; Stow et al., 1995; see supporting information).

Miocene to present-day convergence across the Cyprean subduction zone is also invoked as a mechanism for uplifting and exhuming the mantle peridotites that encompass Mount Olympus (Ring & Pantazides, 2019). These authors downplay the role of serpentinization in forming the Troodos Massif, and favor a west-east elongate doubly plunging anticline with a serpentinite core formed in response to gradual differential shortening. Differential uplift between the Troodos Mantle Sequence and the remaining ocean crustal sequences is proposed to result from the underthrusting of the Eratosthenes seamount (Ring & Pantazides, 2019). This proposed uplift mechanism presents the Troodos Mantle Sequence as a homogenous monolith and does not account for the long-standing subdivision into two separate discrete domains, including evidence that the peridotites from these domains originate from different mantle sources (Batanova & Sobolev, 2000).

7.3. A Unified Model for the Uplift of the Troodos Mantle Sequence

Initiation of significant uplift of the Troodos ophiolite is dated as latest Messinian to Early Pliocene (~5.5 Myr). Decoupling between the Olympus diapir and the regionally uplifted "in-situ" mantle peridotites of the Troodos ophiolite has resulted in at least >3,600 m of differential uplift, transporting mantle peridotites to 1,952 m absl (Figure 8). Unroofing and erosion of the first ultramafic clasts are interpreted to have occurred in the Early Pleistocene, suggesting significant peridotite relief has occurred since then (Figure 8). Once transported to high altitudes, increased rainfall results in the incursion of meteoric water (Figure 8), driving the coupling of deformation-alteration-recrystallization positive-feedback mechanisms of the intensely deformed Artemis diapir. The resulting lower density and easily erodible material induce a secondary decoupling that separates the lower density Artemis diapir from the Olympus diapir (Figure 8), in consequence, differential uplift and exhumation occurs between the Artemis diapir and the Olympus diapir.

7.4. Application of the Mechanistic Uplift Model to Other Settings

Here, we explore whether our simple 1-D mechanistic uplift model is unique to the Troodos Massif or whether it can be applied to a range of other terrestrial and submarine settings including St. Peter and St. Paul Rocks, New Idria Massif, California, Site 637 on the West Iberian Margin, and Macquarie Island.

7.4.1. St. Peter and St. Paul Rocks

The St. Peter and St. Paul Rocks are interpreted as a partially serpentinized serpentinite diapir (e.g., Campos et al., 2005, 2010). Recent interpretation of new bathymetry, seismic, and gravity data sets proposed that the St. Peter and St. Paul Rocks uplifted in response to a ~10 Myr period of transpression at the transform boundary (Maia et al., 2016). They conclude that the present convergence rates at stepovers and transpressive segments are sufficient to uplift the North Ridge Massif some ~3,500 m (Maia et al., 2016). However, a gravity anomaly on the southern flank of the massif indicates the presence of a large low-density layer. This is interpreted to be a ~25-km-thick zone of serpentinized mantle, the base of which approximately coincides with the estimated depth of the 500°C isotherm (Maia et al., 2016).

To establish whether isostatic uplift in response to partial serpentinization reactions can contribute to the overall uplift of the peridotite massif, we apply the mechanistic uplift model (with reasonable parameters; see supporting information) to the St. Peter and St. Paul Rocks. Calculations indicate that partial serpentinization (~40%) of a body in response to a serpentinization front advancing at an average rate of 2,000 m/Myr, will isostatically uplift rock a total of ~3,500 m in the required time frame (10 Myr; Maia et al., 2016),

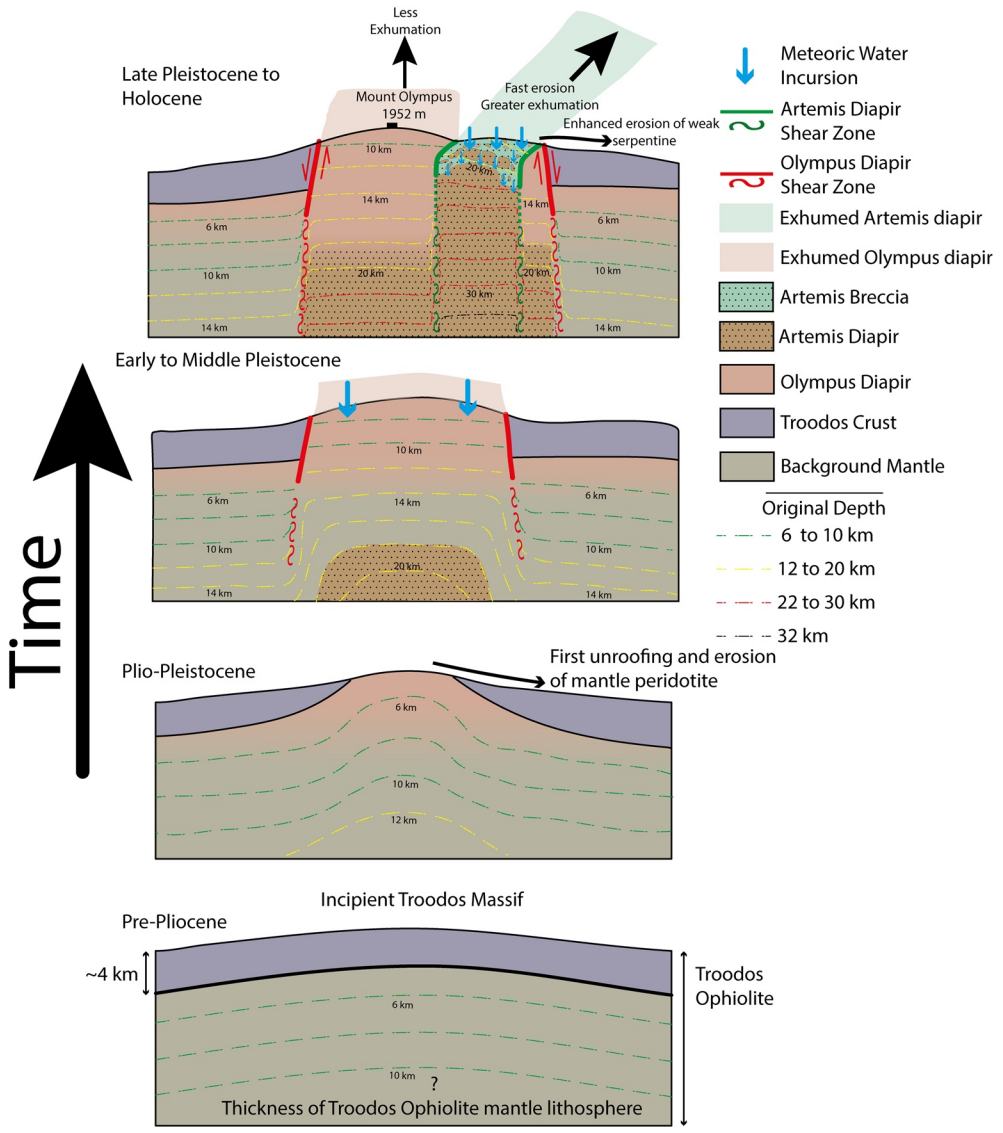

Figure 8. A schematic illustration of our uplift model for the Troodos Mantle Sequence Model highlights the temporal evolution within the Troodos Mantle Sequence culminating in differential serpentinite diapirism and exhumation resulting from contrasting serpentinization styles between both diapiric domains.

generating a body of moderate density (2,800 kg/m^3) that is ~23 km in total thickness (see supporting information), in broad agreement with published interpretation of the gravity data (Maia et al., 2016).

7.4.2. New Idria Serpentinite Diapir

The moderately elevated (1,605 m; prominence 1,061 m) New Idria serpentinite diapir is primarily composed of easily erodible, sheared and crushed, incohesive low-density serpentinite breccia (Coleman, 1996; Mumpton & Thompson, 1975). In addition to serpentine, blocks of eclogite are present that are interpreted to have been entrained during diapiric ascent (Tsujimori et al., 2007). Gravity measurements identify a −35 to −55 mGal negative Bouguer gravity anomaly and the New Idria serpentinite is interpreted to be a dome-like body that only extends to ~4 km depth (Byerly, 1966; McPhee et al., 2004). The gravity anomaly coincides with a strong magnetic signature (~210 nT; McPhee et al., 2004). The emergence of the New Idria serpentinite diapir is dated as Mid-Miocene (~12–~14 Ma) from the presences of detrital chrysotile serpentine in the Big Blue Formation (Casey & Dickinson, 1976; Coleman, 1996; Vermeesch et al., 2006) and continued serpentinite extrusion occurred throughout the Plio-Pleistocene (Coleman, 1996). Application

of the Artemis model parameters (Table 3) to the New Idria setting, suggests that an advancing serpentinization front of 3,000 m/Myr may isostatically produce and maintain an elevation of ~1,000 m in response to a ~4000-m-thick low-density body (see supporting information). These results are in agreement with geophysical constraints and suggest that isostatic uplift due to serpentinization may produce and maintain a serpentinite body of moderate elevation, coincidently generating significant differential uplift and exhumation relative to the surrounding area.

7.4.3. ODP Leg 103 Site 637

To the west of the Galicia Bank on the Iberian Margin, ODP Site 647 ("5100 m Hill") is a ~5-km-wide domal serpentinite protrusion, where strongly altered and completely serpentinized plagioclase-bearing subcontinental mantle rocks are uplifted some ~350 m above the surrounding seafloor (Boillot et al., 1988). Late Miocene sediments unconformably overlay, eroded strongly altered and brecciated serpentinized clasts that transition to strongly altered and brecciated serpentinites with increasing depth (Boillot et al., 1988; Evans & Baltuck, 1988). This exhumed peridotite is an elevated basement high, along an inferred ~70 km wide, ~250 km long peridotite ridge, organized into a series of broadly N-S orientated margin parallel segments, some of which extend over tens of kilometers, and generally denote the ocean-continental crust boundary (e.g., Beslier et al., 1993; Henning et al., 2004; Minshull et al., 2014; Whitmarsh et al., 1996). Recent three-dimensional imaging of serpentinized peridotite bodies along the West Iberian Margin shows that the volume of serpentinized peridotite is related to the amount of displacement along each fault, the implication being that serpentinization occurs when these large brittle normal faults are active (Bayrakci et al., 2016). In response to the penetration of seawater into the mantle along normal faults, isostatic uplift as a result of density reduction from serpentinization reactions is likely to have occurred. Strongly serpentinized (>75%) mantle peridotites are estimated from seismic data to occur on top of the basement with the extent of serpentinization decreasing to <25%–~2 km below (Minshull et al., 2014). The depth of the unaltered mantle is estimated at ~7.5 km below seafloor (Minshull et al., 2014). Lateral and vertical variations in the extent of serpentinization likely resulted in differing magnitudes of isostatic uplift. For example, if we assume the completely serpentinized peridotites recovered from Site 637 extend to ~2 km depth and have average bulk densities of 2,400 kg/m^3 and these rocks overlay a body of partly serpentinized peridotites of moderate density (2,900 kg/m^3) the resulting isostatic uplift due to serpentinization would be ~350 m. This amount of uplift is equivalent to the relative difference in elevation between the summit of Site 637 and the surrounding seafloor.

7.4.4. Macquarie Island

Macquarie Island is a small (34-km long, 5.5-km wide) subantarctic island that is broadly equidistant from Tasmania, New Zealand, and Antarctica (Selkirk et al., 1990) and is the only subaerial exposure of the Macquarie Ridge Complex, a region of shallow bathymetry along the Australian-Pacific plate boundary that runs 1,800 km from the southern extent of the Alpine Fault, New Zealand to the Indo-Pacific-Antarctic plate triple junction (Massell et al., 2000). Transpression along the Macquarie Island section of the Macquarie Ridge Complex is invoked to have uplifted and exposed a coherent section of ocean crust and associated upper mantle rocks (Selkirk et al., 1990). These rocks are in faulted contact with subhorizontal pillow lava flows that make up most of the island. The Finch-Langdon Fault that juxtaposes the lava flows and the titled but continuous upper mantle-lower crustal sequence has been interpreted to be an ocean ridge feature (Rivizzigno & Karson, 2004; Wertz et al., 2003). There is no metamorphic sole on Macquarie Island and nor does the geology present evidence for serpentinite diapirism (e.g., Goscombe & Everard, 1998).

Application of the Olympus domain mechanistic uplift model parameters of this study to this Macquarie Island setting suggests that ~400 m of uplift may be generated in response to an average serpentinization front rate of 3,000 m/Myr since the subaerial emergence of the island (~0.65 Ma; Adamson et al., 1996). Despite the extent of serpentinization and general structure of the rocks beneath Macquarie island being poorly constrained, these estimations suggest the resulting isostatic response may produce substantial uplift if localized serpentinization beneath the Macquarie island section of the Macquarie Ridge Complex has occurred. Although there may be other outcrops of serpentinized ultramafic rocks along the Macquarie Ridge Complex (e.g., Watkins & Gunn, 1971), serpentinization-induced isostatic uplift of Macquarie Island may be an additional contribution, overprinted onto the overall uplift trajectory of island, coincidentally generating the only sub-aerial portion along this transpressive plate boundary.

7.4.5. Wider Implications of the Mechanistic Uplift Model

Application of our 1-D mechanistic uplift model to other settings suggests that it may be applied universally across the spectrum of serpentinite diapirism occurrence. Calculations from previously reported examples of serpentinite diapirism and Macquarie Island suggest that the required amount of surface uplift to form their respective topographic relief, in the constrained timeframe, may be generated exclusively through serpentinization reactions. Manifestations of serpentinization may therefore synchronously induce isostatic uplift. In each of the serpentinized massif settings considered, the overall uplift budget is an interplay between the relative contributions of isostatic uplift and tectonic uplift. For example, for the New Idria Massif the isostatic contribution dominates the overall uplift budget (~4 mm/yr diapiric uplift rate vs. regional ~1 mm/yr tectonic uplift rate; Coleman, 1996; Page et al., 1998). In contrast, for the Macquarie Ridge dynamic tectonic uplift is the principal source of uplift with potentially a secondary minor component of isostatic uplift resulting from serpentinization reactions that have led to the exposure of Macquarie Island.

8. Conclusions

1. Contrasting serpentinization styles are manifest as two distinct serpentinite diapirs within the Troodos ophiolite: (a) a region where the partial hydration of primary minerals results in a strongly serpentinized yet competent and cohesive diapir of moderate density (2,686 ± 83 kg/m^3), here termed the Olympus diapir; and (b) the completely serpentinized Artemis diapir that is composed of an intensely deformed, weak and friable block-clast-breccia-gouge assemblage of low density (1,949 ± 47 kg/m^3) that results from the positive feedback between coupled deformation-alteration-recrystallization.
2. Density reduction and coincident volume expansion resulting from serpentinization reactions induce serpentinite diapirism combined with isostatic uplift transporting and protruding mantle peridotites to high altitude (1,952 m). Calculations from isostatic uplift and differential erosion modeling suggest that mountains akin to Mount Olympus (~2,000 m asl) may form exclusively through serpentinization within the required time frame (~5.5 Myr). The CY-4 drill hole geometry indicates that differential uplift of at least >3.6 km has occurred due to the decoupling between the Olympus diapir and the regional "in-situ" mantle peridotites.
3. The occurrence of mantle peridotites forming the highest elevations of the Troodos Mountains results in strong precipitation, leading to the ingression of meteoric water, as highlighted by oxygen and hydrogen stable isotope analyses. Activation of coupled mechanisms within the Artemis diapir form the low density (1,568 ± 71 kg/m^3), weak, serpentinite gouge end member; increasing the total exhumation (>3.6–~17.5 km) and localization of Artemis' deep materials (Batanova & Sobolev, 2000). Despite greater exhumation occurring within the Artemis diapir, the competent cohesive partially serpentinized peridotites of the Olympus diapir form the regional summit (Mount Olympus, 1,952 m) rather than the weaker deeper materials of the Artemis diapir.
4. Our 1-D mechanistic uplift model for the Troodos Massif is broadly applicable to a spectrum of other protrusions of serpentinized mantle peridotite. Isostatic uplift is an inevitable manifestation of serpentinization reactions that result in density reduction and concomitant volume expansion. For each serpentinized massif, the overall uplift budget will be a combination between the relative contributions of isostatic uplift and dynamic tectonic uplift that jointly contribute to the overall uplift and exposure of serpentinized massifs.

Acknowledgments
The authors gratefully thank the Geological Survey Department of Cyprus for their support (MoU/Ref. No. 05.26.001/5). The authors also thank Dan Doran and Matt Beverley-Smith at the University of Southampton for the preparation of thin sections. Aled D. Evans acknowledges a Natural Environmental Research Council–SPITFIRE CASE PhD award NE/L002531/1 (Natural History Museum CASE partner). Damon A. H. Teagle acknowledges a Royal Society Wolfson Research Merit Award (WM130051). We thank Alastair Robertson for discussions about the uplift and exposure of the Troodos mountains.

Data Availability Statement

All data used within this study are provided and cited accordingly. Previous oxygen and hydrogen stable isotope values are from Heaton (1976), Magaritz and Taylor (1974), and Nuriel et al. (2009).

References

Adamson, D. A., Selkirk, P. M., Price, D. M., Ward, N., & Selkirk, J. M. (1996). Pleistocene uplift and palaeoenvironments of Macquarie Island: Evidence from palaeobeaches and sedimentary deposits. *Papers and Proceedings of the Royal Society of Tasmania*, *130*(2), 25–32. https://doi.org/10.26749/rstpp.130.2.25

Alt, J. C., & Shanks, W. C., III. (2006). Stable isotope compositions of serpentinite seamounts in the Mariana forearc: Serpentinization processes, fluid sources and sulfur metasomatism. *Earth and Planetary Science Letters*, *242*(3–4), 272–285. https://doi.org/10.1016/j.epsl.2005.11.063

Arai, S. (1994). Characterization of spinel peridotites by olivine-spinel compositional relationships: Review and interpretation. *Chemical Geology*, *113*(3–4), 191–204. https://doi.org/10.1016/0009-2541(94)90066-3

Batanova, V. G., & Sobolev, A. V. (2000). Compositional heterogeneity in subduction-related mantle peridotites, Troodos Massif, Cyprus. *Geology*, *28*(1), 55–58. https://doi.org/10.1130/0091-7613(2000)028<0055:chisrm>2.3.co;2

Bayrakci, G., Minshull, T. A., Sawyer, D. S., Reston, T. J., Klaeschen, D., Papenberg, C., et al. (2016). Fault-controlled hydration of the upper mantle during continental rifting. *Nature Geoscience*, *9*(5), 384–388. https://doi.org/10.1038/ngeo2671

Beslier, M. O., Ask, M., & Boillot, G. (1993). Ocean-continent boundary in the Iberia Abyssal Plain from multichannel seismic data. *Tectonophysics*, *218*(4), 383–393. https://doi.org/10.1016/0040-1951(93)90327-g

Birch, F. (1961). The velocity of compressional waves in rocks to 10 kilobars: 2. *Journal of Geophysical Research*, *66*(7), 2199–2224. https://doi.org/10.1029/jz066i007p02199

Birch, F. (1964). Density and composition of mantle and core. *Journal of Geophysical Research*, *69*(20), 4377–4388. https://doi.org/10.1029/jz069i020p04377

Boillot, G., Girardeau, J., & Kornprobst, J. (1988). Rifting of the Galicia margin: Crustal thinning and emplacement of mantle rocks on the seafloor. In G. Boillot, E. L. Winterer, et al. (Eds.), *Proc. ODP, Sci. Results* (Vol. 103, pp. 741–756). College Station, Texas: Ocean Drilling Program. https://doi.org/10.2973/odp.proc.sr.103.179.1988

Boillot, G., Grimaud, S., Mauffret, A., Mougenot, D., Kornprobst, J., Mergoil-Daniel, J., & Torrent, G. (1980). Ocean-continent boundary off the Iberian margin: A serpentinite diapir west of the Galicia Bank. *Earth and Planetary Science Letters*, *48*(1), 23–34. https://doi.org/10.1016/0012-821x(80)90166-1

Bonatti, E. (1976). Serpentinite protrusions in the oceanic crust. *Earth and Planetary Science Letters*, *32*(2), 107–113. https://doi.org/10.1016/0012-821x(76)90048-0

Bonatti, E. (1978). Vertical tectonism in oceanic fracture zones. *Earth and Planetary Science Letters*, *37*(3), 369–379. https://doi.org/10.1016/0012-821x(78)90052-3

Boronina, A., Balderer, W., Renard, P., & Stichler, W. (2005). Study of stable isotopes in the Kouris catchment (Cyprus) for the description of the regional groundwater flow. *Journal of Hydrology*, *308*(1–4), 214–226. https://doi.org/10.1016/j.jhydrol.2004.11.001

Byerly, P. E. (1966). Interpretations of gravity data from the central Coast Ranges and San Joaquin Valley, California. *The Geological Society of America Bulletin*, *77*(1), 83–94. https://doi.org/10.1130/0016-7606(1966)77[83:iogdft]2.0.co;2

Campos, T. F., Bezerra, F. H., Srivastava, N. K., Vieira, M. M., & Vita-Finzi, C. (2010). Holocene tectonic uplift of the St Peter and St Paul Rocks (Equatorial Atlantic) consistent with emplacement by extrusion. *Marine Geology*, *271*(1–2), 177–186. https://doi.org/10.1016/j.margeo.2010.02.013

Campos, T. F., Neto, J. V., Srivastava, N. K., Petta, R. A., Hartmann, L. A., Moraes, J. F. S., et al. (2005). Saint Peter and Saint Paul's archipelago—Tectonic uplift of infra-crustal rocks in the Atlantic Ocean. *Geological and Paleontological Sites of Brazil*. Retrieved from http://sigep.cprm.gov.br/sitio002/sitio002english.pdf

Cao, W., & Paterson, S. (2016). A mass balance and isostasy model: Exploring the interplay between magmatism, deformation and surface erosion in continental arcs using central Sierra Nevada as a case study. *Geochemistry, Geophysics, Geosystems*, *17*(6), 2194–2212. https://doi.org/10.1002/2015gc006229

Casey, T. A. L., & Dickinson, W. R. (1976). Sedimentary serpentinite of the Miocene Big Blue Formation near Cantua Creek, California. *AAPG-SEPM-SEG Pacific Sections Meeting*, *60*(12), 2177. https://doi.org/10.1306/c1ea3ae1-16c9-11d7-8645000102c1865d

Coleman, R. G. (1996). New Idria serpentinite: A land management dilemma. *Environmental and Engineering Geoscience*, *2*(1), 9–22. https://doi.org/10.2113/gseegeosci.ii.1.9

Craw, D., Landis, C. A., & Kelsey, P. I. (1987). Authigenic chrysotile formation in the matrix of Quaternary debris flows, northern Southland, New Zealand. *Clays and Clay Minerals*, *35*(1), 43–52. https://doi.org/10.1346/CCMN.1987.0350106

Darwin, C. R. (1835). *Extracts from letters addressed to Professor Henslow by C. Darwin, Esq: Read at a meeting of the society on the 16th of November 1835*. University Press for the Cambridge Philosophical Society.

Dick, H. J., & Bullen, T. (1984). Chromian spinel as a petrogenetic indicator in abyssal and alpine-type peridotites and spatially associated lavas. *Contributions to Mineralogy and Petrology*, *86*(1), 54–76. https://doi.org/10.1007/bf00373711

Dickinson, W. R. (1966). Table Mountain serpentinite extrusion in California Coast ranges. *Geological Society of America Bulletin*, *77*(5), 451–472. https://doi.org/10.1130/0016-7606(1966)77[451:tmseic]2.0.co;2

Ergün, M., Okay, S., Sari, C., Oral, E. Z., Ash, M., Hall, J., & Miller, H. (2005). Gravity anomalies of the Cyprus Arc and their tectonic implications. *Marine Geology*, *221*(1–4), 349–358. https://doi.org/10.1016/j.margeo.2005.03.004

Evans, C. A., & Baltuck, M. (1988). Low-temperature alteration of peridotite, Hole 637A. In G. Boillot, E. L. Winterer, et al. (Eds.), *Proc. ODP, Sci. Results* (Vol. 103, pp. 235–239). College Station, Texas: Ocean Drilling Program. https://doi.org/10.2973/odp.proc.sr.103.139.1988

Feld, C., Mechie, J., Huebscher, C., Hall, J., Nicolaides, S., Gurbuz, C., et al. (2017). Crustal structure of the Eratosthenes Seamount, Cyprus and S. Turkey from an amphibian wide-angle seismic profile. *Tectonophysics*, *700*, 32–59. https://doi.org/10.1016/j.tecto.2017.02.003

Follows, E. J. (1990). *Sedimentology and tectonic setting of Miocene reef and related sediments in Cyprus (PhD Thesis)*. University of Edinburgh.

Fossen, H., & Cavalcante, G. C. G. (2017). Shear zones—A review. *Earth-Science Reviews*, *171*, 434–455. https://doi.org/10.1016/j.earscirev.2017.05.002

Fryer, P. (2012). Serpentinite mud volcanism: Observations, processes, and implications. *Annual Review of Marine Science*, *4*, 345–373. https://doi.org/10.1146/annurev-marine-120710-100922

Fryer, P., Ambos, E. L., & Hussong, D. M. (1985). Origin and emplacement of Mariana forearc seamounts. *Geology*, *13*(11), 774–777. https://doi.org/10.1130/0091-7613(1985)13<774:oaeomf>2.0.co;2

Fryer, P., Pearce, J. A., & Stokking, L. B. (1992). A synthesis of Leg 125 drilling of serpentine seamounts on the Mariana and Izu–Bonin forearcs. In P. Fryer, J. A. Pearce, L. B. Stokking, et al. (Eds.), *Proc. ODP, Sci. Results* (Vol. 125, pp. 445–485). College Station, Texas: Ocean Drilling Program. https://doi.org10.2973/odp.proc.sr.125.168.1992

Gass, I. G. (1968). Is the Troodos massif of Cyprus a fragment of Mesozoic ocean floor? *Nature*, *220*(5162), 39–42. https://doi.org/10.1038/220039a0

Gass, I. G. (1977). *Origin and emplacement of ophiolites* (Vol. 7, pp. 72–76). London: Geological Society, Special Publications. https://doi.org/10.1144/gsl.sp.1977.007.01.07

Gass, I. G., & Masson-Smith, D. (1963). The geology and gravity anomalies of the Troodos Massif, Cyprus. *Philosophical Transactions of the Royal Society of London - Series A: Mathematical and Physical Sciences*, *255*(1060), 417–467. https://doi.org/10.1098/rspb.1963.003010.1098/rsta.1963.0009

Goscombe, B. D., & Everard, J. L. (1998). *1: 10000 geological map of Macquarie island*. Mineral Resources Tasmania.

Hacker, B. R., Mosenfelder, J. L., & Gnos, E. (1996). Rapid emplacement of the Oman ophiolite: Thermal and geochronologic constraints. *Tectonics*, *15*(6), 1230–1247. https://doi.org/10.1029/96tc01973

Heaton, T. H. E. (1976). *Hydrogen and oxygen isotope study of the metamorphism and mineralisation of the Troodos Complex, Cyprus (PhD Thesis)*. University of Edinburgh.

Heaton, T. H. E., & Sheppard, S. M. F. (1977). *Hydrogen and oxygen isotope evidence for sea-water-hydrothermal alteration and ore deposition, Troodos Complex, Cyprus* (Vol. 7, pp. 42–57). London: Geological Society, Special Publications. https://doi.org/10.1144/gsl.sp.1977.007.01.05

Hekinian, R., Juteau, T., Gracia, E., Sichler, B., Sichel, S., Udintsev, G., et al. (2000). Submersible observations of Equatorial Atlantic Mantle: The St. Paul fracture zone region. *Marine Geophysical Researches*, *21*(6), 529–560. https://doi.org/10.1023/a:1004819701870

Henning, A. T., Sawyer, D. S., & Templeton, D. C. (2004). Exhumed upper mantle within the ocean-continent transition on the northern West Iberia margin: Evidence from prestack depth migration and total tectonic subsidence analyses. *Journal of Geophysical Research*, *109*(B5). https://doi.org/10.1029/2003jb002526

Hess, H. H. (1954). Geological hypotheses and the earth's crust under the oceans. *Proceedings of the Royal Society of London—Series A: Mathematical and Physical Sciences*, *222*, 341–348. https://doi.org/10.1098/rspa.1954.0077

Hyndman, R. D., & Drury, M. J. (1976). The physical properties of oceanic basement rocks from deep drilling on the Mid-Atlantic Ridge. *Journal of Geophysical Research*, *81*(23), 4042–4052. https://doi.org/10.1029/jb081i023p04042

Ishii, T., Robinson, P. T., Maekawa, H., & Fiske, R. (1992). Petrological studies of peridotites from diapiric serpentinite seamounts in the Izu-Ogasawara-Mariana forearc, Leg 125. In P. Fryer, J. A. Pearce, L. B. Stokking, et al. (Eds.), *Proc. ODP, Sci. Results* (Vol. 125, pp. 445–485). College Station, Texas: Ocean Drilling Program. https://doi.org/10.2973/odp.proc.sr.125.129.1992

Kelemen, P. B., Matter, J., Streit, E. E., Rudge, J. F., Curry, W. B., & Blusztajn, J. (2011). Rates and mechanisms of mineral carbonation in peridotite: Natural processes and recipes for enhanced, in situ CO_2 capture and storage. *Annual Review of Earth and Planetary Sciences*, *39*, 545–576. https://doi.org/10.1146/annurev-earth-092010-152509

Kil, Y., Lee, S. H., Park, M. H., & Wendlandt, R. F. (2010). Nature of serpentinization of ultramafic rocks from Hero Fracture Zone, Antarctic: Constraints from stable isotopes. *Marine Geology*, *274*(1–4), 43–49. https://doi.org/10.1016/j.margeo.2010.03.004

Kyser, T. K., & Kerrich, R. (1991). Retrograde exchange of hydrogen isotopes between hydrous minerals and water at low temperatures. In H. P. Taylor, J. R. O'Neil, & I. Kaplan (Eds.), *Stable Isotope Geochemistry: A Tribute to Samuel Epstein* (Vol. 3, pp. 409–424). Geochemical Society Special Publication.

Kyser, T. K., O'Hanley, D. S., & Wicks, F. J. (1999). The origin of fluids associated with serpentinization; evidence from stable-isotope compositions. *The Canadian Mineralogist*, *37*(1), 223–237.

Lamadrid, H. M., Rimstidt, J. D., Schwarzenbach, E. M., Klein, F., Ulrich, S., Dolocan, A., & Bodnar, R. J. (2017). Effect of water activity on rates of serpentinization of olivine. *Nature Communications*, *8*(1), 1–9. https://doi.org/10.1038/ncomms16107

Lee, C. T. A., Thurner, S., Paterson, S., & Cao, W. (2015). The rise and fall of continental arcs: Interplays between magmatism, uplift, weathering, and climate. *Earth and Planetary Science Letters*, *425*, 105–119. https://doi.org/10.1016/j.epsl.2015.05.045

Lowell, R. P., & Rona, P. A. (2002). Seafloor hydrothermal systems driven by the serpentinization of peridotite. *Geophysical Research Letters*, *29*(11). https://doi.org/10.1029/2001gl014411

Macdonald, A. H., & Fyfe, W. S. (1985). Rate of serpentinization in seafloor environments. *Tectonophysics*, *116*(1–2), 123–135. https://doi.org/10.1016/0040-1951(85)90225-2

Mackenzie, G. D., Maguire, P. K. H., Coogan, L. A., Khan, M. A., Eaton, M., & Petrides, G. (2006). Geophysical constraints on the crustal architecture of the Troodos ophiolite: Results from the IANGASS project. *Geophysical Journal International*, *167*(3), 1385–1401. https://doi.org/10.1111/j.1365-246x.2006.03144.x

MacLeod, C. J. (1988). *The tectonic evolution of the Eastern Limassol Forest Complex, Cyprus (PhD Thesis)*. The Open University.

MacLeod, C. J. (1990). Role of the Southern Troodos Transform Fault in the rotation of the Cyprus microplate: evidence from the Eastern Limassol Forest Complex. In J. Malpas, E. M. Moores, A. Panayiotou, & C. Xenophontos (Eds.), *Ophiolites: Ocean Crustal Analogues, Proc. Symp. 'TROODOS 1987'* (pp. 75-85). Nicosia, Cyprus: Geological Survey Department.

Magaritz, M., & Taylor, H. P., Jr. (1974). Oxygen and hydrogen isotope studies of serpentinization in the Troodos ophiolite complex, Cyprus. *Earth and Planetary Science Letters*, *23*(1), 8–14. https://doi.org/10.1016/0012-821x(74)90023-5

Maia, M., Sichel, S., Briais, A., Brunelli, D., Ligi, M., Ferreira, N., et al. (2016). Extreme mantle uplift and exhumation along a transpressive transform fault. *Nature Geoscience*, *9*(8), 619–623. https://doi.org/10.1038/ngeo2759

Malpas, J., Robinson, P. T., & Salisbury, M. (1989). Geology and geophysics of borehole CY-4 of the Cyprus crustal study project, summary. In I. L. Gibson, J. Malpas, P. T. Robinson, & C. Xenophontos (Eds.), *Cyprus crustal study project Initial Rep. Hole CY-4* (pp. 381–393).

Martin, B., & Fyfe, W. S. (1970). Some experimental and theoretical observations on the kinetics of hydration reactions with particular reference to serpentinization. *Chemical Geology*, *6*, 185–202. https://doi.org/10.1016/0009-2541(70)90018-5

Massell, C., Coffin, M. F., Mann, P., Mosher, S., Frohlich, C., Duncan, C. S., et al. (2000). Neotectonics of the Macquarie Ridge Complex, Australia-Pacific plate boundary. *Journal of Geophysical Research*, *105*(B6), 13457–13480. https://doi.org/10.1029/1999jb900408

McCallum, J. E. (1989). *Sedimentation and tectonics of the Plio-Pleistocene of Cyprus (PhD Thesis)*. University of Edinburgh.

McCollom, T. M., Klein, F., Robbins, M., Moskowitz, B., Berquó, T. S., Jöns, N., et al. (2016). Temperature trends for reaction rates, hydrogen generation, and partitioning of iron during experimental serpentinization of olivine. *Geochimica et Cosmochimica Acta*, *181*, 175–200. https://doi.org/10.1016/j.gca.2016.03.002

McPhee, D. K., Jachens, R. C., & Wentworth, C. M. (2004). Crustal structure across the San Andreas Fault at the SAFOD site from potential field and geologic studies. *Geophysical Research Letters*, *31*(12). https://doi.org/10.1029/2003gl019363

Melson, W. G., Hart, S. R., & Thompson, G. (1972). St. Paul's rocks, equatorial Atlantic: Petrogenesis, radiometric ages and implications on sea-floor spreading. In R. Shagam, R. B. Hargraves, W. J. Morgan, F. B. Van Houten, C. A. Burk, H. D. Holland, & L. C. Hollister (Eds.), *Studies in Earth and space sciences: A memoir in honor of Harry Hammond Hess* (Vol. 132, pp. 241–272). Geological Society of America. https://doi.org/10.1130/mem132-p241

Minshull, T. A., Dean, S. M., & Whitmarsh, R. B. (2014). The peridotite ridge province in the southern Iberia Abyssal Plain: Seismic constraints revisited. *Journal of Geophysical Research: Solid Earth*, *119*(3), 1580–1598. https://doi.org/10.1002/2014jb011011

Moore, D. E., & Rymer, M. J. (2007). Talc-bearing serpentinite and the creeping section of the San Andreas fault. *Nature*, *448*(7155), 795–797. https://doi.org/10.1038/nature06064

Moores, E. M., Robinson, P. T., Malpas, J., & Xenophonotos, C. (1984). Model for the origin of the Troodos massif, Cyprus, and other mideast ophiolites. *Geology*, *12*(8), 500–503. https://doi.org/10.1130/0091-7613(1984)12<500:mftoot>2.0.co;2

Moores, E. M., & Vine, F. J. (1971). The Troodos Massif, Cyprus and other ophiolites as oceanic crust: Evaluation and implications. *Philosophical Transactions of the Royal Society of London—Series A: Mathematical and Physical Sciences*, *268*(1192), 443–467. https://doi.org/10.1098/rsta.1971.0006

Morag, N., Haviv, I., & Katzir, Y. (2016). From ocean depths to mountain tops: Uplift of the Troodos ophiolite (Cyprus) constrained by low-temperature thermochronology and geomorphic analysis. *Tectonics*, *35*(3), 622–637. https://doi.org/10.1002/2015tc004069

Mottl, M. J., Wheat, C. G., Fryer, P., Gharib, J., & Martin, J. B. (2004). Chemistry of springs across the Mariana forearc shows progressive devolatilization of the subducting plate. *Geochimica et Cosmochimica Acta*, *68*(23), 4915–4933. https://doi.org/10.1016/j.gca.2004.05.037

Mukasa, S. B., & Ludden, J. N. (1987). Uranium-lead isotopic ages of plagiogranites from the Troodos ophiolite, Cyprus, and their tectonic significance. *Geology*, *15*(9), 825–828. https://doi.org/10.1130/0091-7613(1987)15<825:uiaopf>2.0.co;2

Mumpton, F. A., & Thompson, C. S. (1975). Mineralogy and origin of the Coalinga asbestos deposit. *Clays and Clay Minerals*, *23*(2), 131–143. https://doi.org/10.1346/ccmn.1975.0230209

Murton, B. J. (1986). Anomalous oceanic lithosphere formed in a leaky transform fault: Evidence from the western Limassol Forest Complex, Cyprus. *Journal of the Geological Society*, *143*(5), 845–854. https://doi.org/10.1144/gsjgs.143.5.0845

Nuriel, P., Katzir, Y., Abelson, M., Valley, J. W., Matthews, A., Spicuzza, M. J., & Ayalon, A. (2009). Fault-related oceanic serpentinization in the Troodos ophiolite, Cyprus: Implications for a fossil oceanic core complex. *Earth and Planetary Science Letters*, *282*(1–4), 34–46. https://doi.org/10.1016/j.epsl.2009.02.029

Page, B. M., Coleman, R. G., & Thompson, G. A. (1998). Late Cenozoic tectonics of the central and southern Coast Ranges of California. *The Geological Society of America Bulletin*, *110*(7), 846–876. https://doi.org/10.1130/0016-7606(1998)110<0846:olctot>2.3.co;2

Parkinson, I. J., & Pearce, J. A. (1998). Peridotites from the Izu-Bonin-Mariana forearc (ODP Leg 125): Evidence for mantle melting and melt–mantle interaction in a supra-subduction zone setting. *Journal of Petrology*, *39*(9), 1577–1618. https://doi.org/10.1093/petroj/39.9.1577

Pearce, J. A., Lippard, S. J., & Roberts, S. (1984). *Characteristics and tectonic significance of supra-subduction zone ophiolites* (Vol. 16(1)pp. 77–94). London: Geological Society, Special Publications. https://doi.org/10.1144/gsl.sp.1984.016.01.06

Poole, A. J., & Robertson, A. H. F. (1991). Quaternary uplift and sea-level change at an active plate boundary, Cyprus. *Journal of the Geological Society*, *148*(5), 909–921. https://doi.org/10.1144/gsjgs.148.5.0909

Poole, A. J., & Robertson, A. H. F. (1998). Pleistocene fanglomerate deposition related to uplift of the Troodos Ophiolite, Cyprus. In A. H. F. Robertson, K.-C. Emeis, C. Richter, & A. Camerlenghi (Eds.), *Proc. ODP, Sci. Results* (Vol. 160, pp. 545–566). College Station, Texas: Ocean Drilling Program. https://doi.org/10.2973/odp.proc.sr.160.064.1998

Ramsay, J. (1980). Shear zone geometry: A review. *Journal of Structural Geology*, *2*(1–2), 83–99. https://doi.org/10.1016/0191-8141(80)90038-3

Ring, U., & Pantazides, H. (2019). The uplift of the Troodos Massif, Cyprus. *Tectonics*, *38*(8), 3124–3139. https://doi.org/10.1029/2019tc005514

Rivizzigno, P. A., & Karson, J. A. (2004). Structural expression of oblique seafloor spreading in the Macquarie Island Ophiolite. *Southern Ocean Geology*, *32*(2), 125–128. https://doi.org/10.1130/g19906.1

Robertson, A. H. F. (1977). Tertiary uplift history of the Troodos massif, Cyprus. *Geological Society of America Bulletin*, *88*(12), 1763–1772. https://doi.org/10.1130/0016-7606(1977)88<1763:tuhott>2.0.co;2

Robertson, A. H. F. (1998). Tectonic significance of the Eratosthenes Seamount: A continental fragment in the process of collision with a subduction zone in the eastern Mediterranean (Ocean Drilling Program Leg 160). *Tectonophysics*, *298*(1–3), 63–82. https://doi.org/10.1016/s0040-1951(98)00178-4

Rooney, J. S., Tarling, M. S., Smith, S. A., & Gordon, K. C. (2018). Submicron Raman spectroscopy mapping of serpentinite fault rocks. *Journal of Raman Spectroscopy*, *49*(2), 279–286. https://doi.org/10.1002/jrs.5277

Rouchy, J. M., Orszag-Sperber, F., Blanc-Valleron, M. M., Pierre, C., Rivière, M., Combourieu-Nebout, N., & Panayides, I. (2001). Paleoenvironmental changes at the Messinian–Pliocene boundary in the eastern Mediterranean (southern Cyprus basins): Significance of the Messinian Lago-Mare. *Sedimentary Geology*, *145*(1–2), 93–117. https://doi.org/10.1016/s0037-0738(01)00126-9

Saccocia, P. J., Seewald, J. S., & Shanks, W. C., III. (2009). Oxygen and hydrogen isotope fractionation in serpentine-water and talc-water systems from 250 to 450 C, 50 MPa. *Geochimica et Cosmochimica Acta*, *73*(22), 6789–6804. https://doi.org/10.1016/j.gca.2009.07.036

Schuiling, R. D. (2011). Troodos: A giant serpentinite diapir. *International Journal of Geosciences*, *2*(2), 98–101. https://doi.org/10.4236/ijg.2011.22010

Searle, M., & Cox, J. (1999). Tectonic setting, origin, and obduction of the Oman ophiolite. *Geological Society of America Bulletin*, *111*(1), 104–122. https://doi.org/10.1130/0016-7606(1999)111<0104:tsoaoo>2.3.co;2

Selkirk, P., Seppelt, R., & Selkirk, D. (1990). *Subantarctic Macquarie Island: Environment and biology*. Cambridge University Press.

Shelton, A. W. (1993). Troodos revisited: The Mount Olympus gravity anomaly. *Geological Society, London, Special Publications 76*(1), 197–212. https://doi.org/10.1144/gsl.sp.1993.076.01.09

Simoes, M., Braun, J., & Bonnet, S. (2010). Continental-scale erosion and transport laws: A new approach to quantitatively investigate macroscale landscapes and associated sediment fluxes over the geological past. *Geochemistry, Geophysics, Geosystems*, *11*(9). https://doi.org/10.1029/2010gc003121

Stow, D. A., Braakenburg, N. E., & Xenophontos, C. (1995). The Pissouri Basin fan-delta complex, southwestern Cyprus. *Sedimentary Geology*, *98*(1–4), 245–262. https://doi.org/10.1016/0037-0738(95)00035-7

Thom, J. G., Dipple, G. M., Power, I. M., & Harrison, A. L. (2013). Chrysotile dissolution rates: Implications for carbon sequestration. *Applied Geochemistry*, *35*, 244–254. https://doi.org/10.1016/J.APGEOCHEM.2013.04.016

Toft, P. B., Arkani-Hamed, J., & Haggerty, S. E. (1990). The effects of serpentinization on density and magnetic susceptibility: A petrophysical model. *Physics of the Earth and Planetary Interiors*, *65*(1–2), 137–157. https://doi.org/10.1016/0031-9201(90)90082-9

Tsujimori, T., Liou, J. G., Coleman, R. G., Cloos, M., Carlson, W. D., Gilbert, M. C., & Sorensen, S. S. (2007). *Finding of high-grade tectonic blocks from the New Idria serpentinite body, Diablo Range, California: Petrologic constraints on the tectonic evolution of an active serpentinite diapir*. Geological Society of America.

Vermeesch, P., Miller, D. D., Graham, S. A., De Grave, J., & McWilliams, M. O. (2006). Multimethod detrital thermochronology of the Great Valley Group near New Idria, California. *Geological Society of America Bulletin*, *118*(1–2), 210–218. https://doi.org/10.1130/b25797.1

Watkins, N. D., & Gunn, B. M. (1971). Petrology, geochemistry, and magnetic properties of some rocks dredged from the Macquarie ridge. *New Zealand Journal of Geology and Geophysics*, *14*(1), 153–168. https://doi.org/10.1080/00288306.1971.10422468

Wenner, D. B. (1971). *Hydrogen and oxygen isotopic studies of serpentinization of ultramafic rocks (PhD Thesis)*. California Institute of Technology.

Wenner, D. B., & Taylor, H. P. (1971). Temperatures of serpentinization of ultramafic rocks based on O^{18}/O^{16} fractionation between coexisting serpentine and magnetite. *Contributions to Mineralogy and Petrology*, *32*(3), 165–185. https://doi.org/10.1007/bf00643332

Wertz, K. L., Mosher, S., Daczko, N. R., & Coffin, M. F. (2003). Macquarie Island's Finch-Langdon fault: A ridge-transform inside-corner structure. *Geology*, *31*(8), 661–664. https://doi.org/10.1130/g19441.1

Whitmarsh, R.B., & Sawyer, D. S. (1996). The ocean/continent transition beneath the Iberia abyssal plain and continental-rifting to seafloor-spreading processes. In R. B. Whitmarsh, D. S. Sawyer, A. Klaus, & D. G. Masson (Eds.), *Proc. ODP, Sci. Results* (Vol. 149, pp. 713–733). College Station, Texas: Ocean Drilling Program. https://doi.org/10.2973/odp.proc.sr.149.249.1996

Wilson, R., & Ingham, F. (1959). *The geology of the Xeros-Troodos area (No. 1)*. Authority of the Government of Cyprus.

Zheng, Y. F. (1993). Calculation of oxygen isotope fractionation in hydroxyl-bearing silicates. *Earth and Planetary Science Letters*, *120*(3–4), 247–263. https://doi.org/10.1016/0012-821x(93)90243-3